ANNUAL REVIEWS

Annual Review of Fluid Mechanics

Transition to Turbulence in Pipe Flow

Marc Avila,[1] Dwight Barkley,[2] and Björn Hof[3]

[1]Center of Applied Space Technology and Microgravity (ZARM), University of Bremen, Bremen, Germany

[2]Mathematics Institute, University of Warwick, Coventry, United Kingdom; email: D.Barkley@warwick.ac.uk

[3]Institute of Science and Technology Austria, Klosterneuburg, Austria

Annu. Rev. Fluid Mech. 2023. 55:575–602

First published as a Review in Advance on October 20, 2022

The *Annual Review of Fluid Mechanics* is online at fluid.annualreviews.org

https://doi.org/10.1146/annurev-fluid-120720-025957

Keywords

shear flow, transient growth, turbulent puff, turbulent slug, intermittency, transient chaos, directed percolation

Abstract

Since the seminal studies by Osborne Reynolds in the nineteenth century, pipe flow has served as a primary prototype for investigating the transition to turbulence in wall-bounded flows. Despite the apparent simplicity of this flow, various facets of this problem have occupied researchers for more than a century. Here we review insights from three distinct perspectives: (*a*) stability and susceptibility of laminar flow, (*b*) phase transition and spatiotemporal dynamics, and (*c*) dynamical systems analysis of the Navier—Stokes equations. We show how these perspectives have led to a profound understanding of the onset of turbulence in pipe flow. Outstanding open points, applications to flows of complex fluids, and similarities with other wall-bounded flows are discussed.

1. INTRODUCTION

Reynolds number (*Re*): the *Re* for pipe flow is defined as $Re = UD/\nu$, where U is the mean velocity (also known as the bulk velocity), D is the pipe diameter, and ν is the kinematic viscosity

"What we really cannot do is deal with actual, wet water running through a pipe. That is the central problem which we ought to solve some day, and we have not." This statement by Richard Feynman (Feynman et al. 1963) captures how the seemingly simple motion of fluid through a pipe can present such an immense scientific challenge. The central problem Feynman refers to arises because the fluid flowing through a pipe can become turbulent, and we review here the recent progress on understanding this appearance of turbulence—that is, the transition to turbulence. The term transition can be interpreted in various ways. An engineer may be most interested in the susceptibility of the laminar flow to disturbances and in the corresponding instability threshold as a function of the flow rate (**Figure 1*a***), while a physicist may think of the problem as a phase transition and seek to determine the underlying critical point (**Figure 1*b***), and a mathematician may ask from where solutions other than the laminar state originate, how these subsequently give rise to a chaotic dynamics, and how this dynamics is separated from laminar flow (**Figure 1*c***). In flows that exhibit linear instabilities, such as Rayleigh–Bénard convection or Taylor–Couette flow driven by inner cylinder rotation, the situation is much simpler, as all these questions essentially merge and are covered by the same framework. In pipe flow, in contrast, each aspect requires an entirely different approach. Consequently, there is not just one single answer to the transition problem. In the following, we guide the reader through the different facets of the transition problem for pipe flow, in each case explaining the perspective and goals and what has been learned.

2. EXPERIMENTS

Before delving into the three perspectives on transition, we review some key experimental observations and historically important works. Many of the concepts introduced in this section are developed more fully throughout this review.

2.1. Natural Transition

Although Newtonian pipe flow is solely governed by the Reynolds number (*Re*), in laboratory experiments the first appearance of turbulence can occur over a wide range of *Re*. Reynolds (1883) could shift the onset of turbulence from $Re \approx 2{,}000$ to 13,000 by reducing disturbances at the pipe inlet. In later experiments, flows could be held laminar, even up to $Re = 100{,}000$ (Pfenniger 1961).

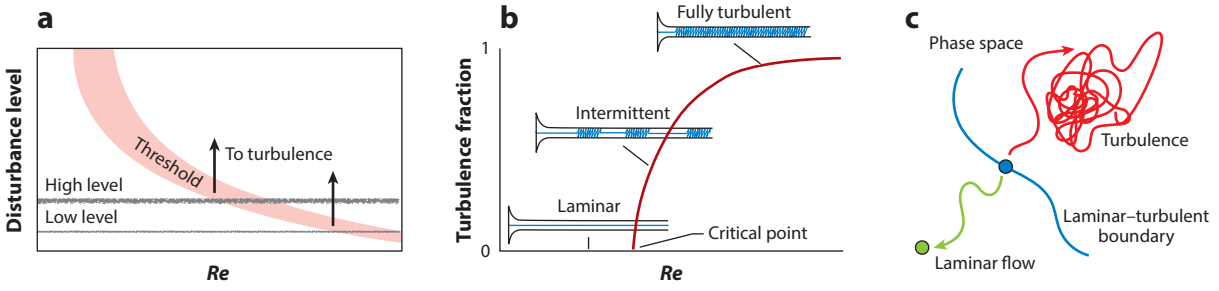

Figure 1

Three perspectives on the transition problem for pipe flow. (*a*) Perspective of susceptibility of linearly stable laminar flow. Small disturbances to laminar flow may trigger a transition to turbulence beyond a certain Reynolds number *Re*, depending on both the level and the form of the disturbance. (*b*) Perspective of phase transitions. Once triggered, turbulence near onset is a spatiotemporally complex phenomenon whose critical behavior can be understood in the context of statistical phase transitions. (*c*) Perspective of the Navier–Stokes equations as a dynamical system. Each point in phase space represents a full velocity field. Trajectories, fixed points, and other sets in phase space provide a detailed understanding of the dynamics of turbulence.

We refer to the natural transition point as the perceived threshold *Re* for the onset of turbulence in a given apparatus.

As discussed in Section 3, laminar Hagen–Poiseuille (HP) flow is stable to infinitesimal perturbations up to very high, and possibly infinite, *Re* (Salwen et al. 1980, Meseguer & Trefethen 2003). Therefore, an initially laminar flow becomes turbulent only as a consequence of perturbations of finite amplitude, something Reynolds himself noted (Reynolds 1883). Because HP flow becomes more susceptible to perturbations with increasing *Re* (see **Figure 1*a***), noise and disturbances must be reduced to avoid transition as *Re* increases. This is particularly true at the pipe entrance, where sophisticated inlet designs, e.g., Wygnanski & Champagne (1973), are needed to realize laminar flow at *Re* significantly exceeding 10,000. Imperfections and disturbance levels differ from one experimental setup to the next, and thus so do the natural transition points.

Even if the entrance flow is held laminar, the profile at high *Re* may deviate significantly from parabolic HP flow. Pipe lengths may be too short to allow the parabolic profile to sufficiently develop. At high *Re*, even very small forces such as the Coriolis force can cause large distortions to the profile (Draad & Nieuwstadt 1998). Consequently, the natural transition point is influenced by many factors, and in principle even flows in two identical experimental setups can become turbulent at considerably different *Re* due to being located at different latitudes or due to small variations between the ambient and the fluid temperature, for example.

Hagen–Poiseuille (HP) flow: fully developed laminar pipe flow. It is steady, purely axial, and of parabolic shape in the radial direction, $\mathbf{U}_{\mathrm{HP}} = U(r)\,\mathbf{e}_z$, where r and z are the radial and axial directions, respectively

Puff: a spatially localized patch of turbulence that maintains nearly constant form and speed as it moves down the pipe. Early works referred to these structures as flashes

2.2. Reynolds Critical Point

Given that the natural transition point strongly depends on the experimental apparatus, Reynolds (1883) proposed a method for determining a reproducible critical point for the onset of turbulence (please see sidebar titled Reynolds Critical Point). Reynolds's idea was to disturb the flow in a controlled manner and then determine whether, sufficiently far downstream, the flow was, or was not, turbulent. This could be used to determine a precise critical *Re* beyond which turbulence is first sustained indefinitely in suitably long pipes. This is a remarkable insight from the nineteenth century since it is exactly how we now understand critical phenomena in systems with a coexisting active state (turbulence) and an absorbing state (stable laminar flow). We address the Reynolds critical point in Section 5.

2.3. Localized and Expanding Turbulence: Puffs and Slugs

At the lowest *Re* for which turbulence can be observed, it appears only in the form of localized patches. Reynolds (1883) referred to these as flashes, but they are now commonly called puffs (see **Figure 2*a*,*c*,*e***). Puffs were observed in early experiments by Rotta (1956) and Lindgren (1957) and were subsequently studied in more detail by Wygnanski & Champagne (1973). Turbulent puffs can be detected experimentally down to *Re* as low as ≈1,500 (Hof et al. 2005). Puffs advect downstream at approximately the bulk flow velocity. They have a well-defined characteristic shape; the

REYNOLDS CRITICAL POINT

Reynolds (1883, pp. 957–58) proposed a definition of the critical point for the onset of turbulence. We quote directly from Reynolds (1883), adding text in brackets as needed for clarity: "if in a tube of sufficient length the water were at first admitted in a high state of disturbance, then as the water proceeded along the tube the disturbance would settle down into a steady condition, which condition would be one of eddies [turbulent flow] or steady motion [laminar flow], according to whether the velocity was above or below what may be called the real critical value."

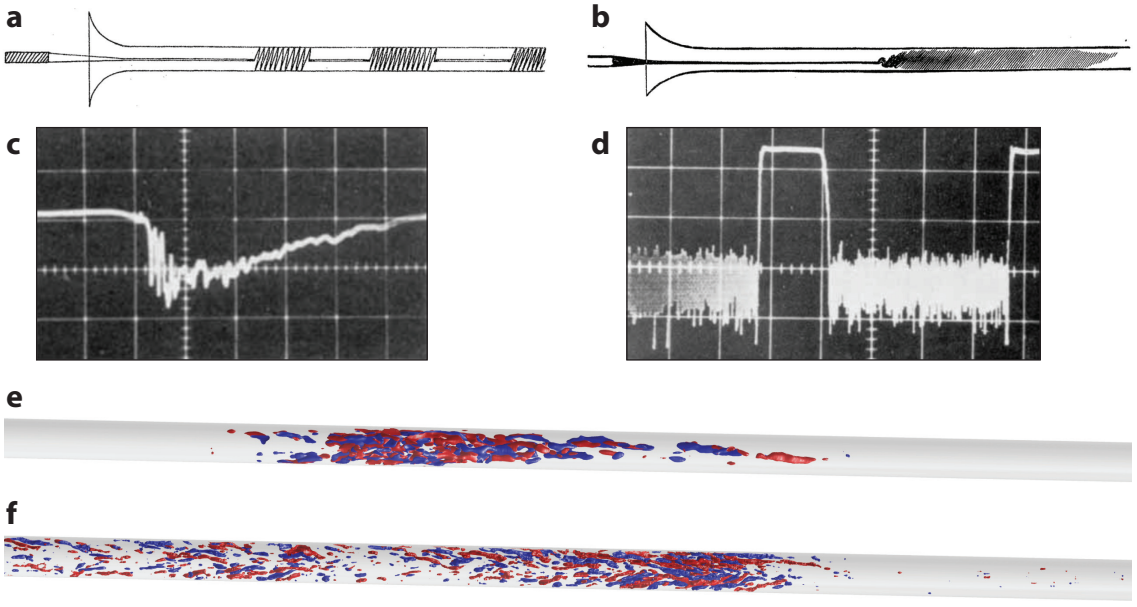

Figure 2

Puffs and slugs. (*a*,*b*) Sketches reprinted from Reynolds (1883). (*c*,*d*) Experimental measurements of centerline velocities reprinted with permission from Wygnanski & Champagne (1973) at (*c*) $Re = 2{,}360$ and (*d*) $Re = 4{,}200$. (*e*,*f*) Streamwise-vorticity contours from optical experimental measurements for $Re = 2{,}000$ and 3,000; images courtesy of Kerstin Avila and Bastian Bäuerlein. Panels *a*, *c*, and *e* correspond to puffs, while panels *b*, *d*, and *f* correspond to the slug regime.

upstream front is marked by a sharp drop of the centerline velocity, while downstream the centerline velocity gradually recovers to the laminar value (**Figure 2*c***). With increasing *Re*, turbulence delocalizes, and puffs give way to expanding patches of turbulence known as slugs (Wygnanski & Champagne 1973, Darbyshire & Mullin 1995) (see **Figure 2*b*,*d*,*f***). Unlike puffs, the size of a turbulent slug is determined by the perturbation that generated it and how long it has evolved since its generation.

Further details on puffs and slugs appear throughout this review. They are historically important, and moreover, it is impossible to discuss the transition to turbulence in pipe flow without introducing these structures from the outset. The dynamics of puffs is crucial to determining the Reynolds critical point, as we see in Section 5.

Slug: a spatially expanding patch of turbulence that leads to an overall increase in the amount of turbulence within the flow

Intermittency factor γ: the fraction of time, at a fixed spatial location, that a flow is in the turbulent state

2.4. Perturbation Schemes

Employing perturbations to obtain reproducible behavior in experiments raises the questions of how to most efficiently disturb the flow and whether the choice of disturbance type affects the resulting flow states.

2.4.1. Continuous perturbations. Early experiments commonly used fixed static disturbance, such as an orifice, at the pipe entrance. Such perturbations produced more consistent results than those for natural transition, but they remain far from converging to the true critical velocity anticipated by Reynolds (see Mukund & Hof 2018 for a discussion of suggested critical points). **Figure 3** shows experimental results by Rotta (1956) obtained using an orifice disturbance. The intermittency factor γ, which quantifies the fraction of the flow that is turbulent, depends on the measurement location along the pipe. With increasing downstream position, the amount of

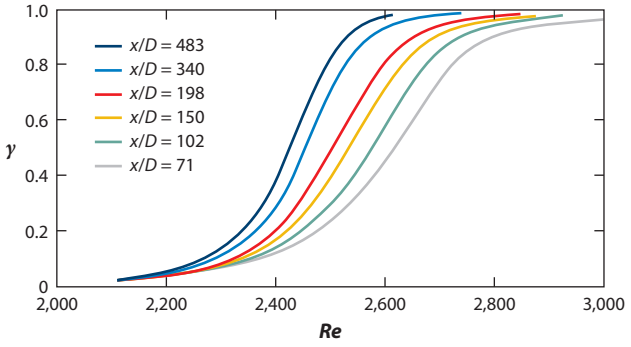

Figure 3

Intermittency factor γ as a function of Reynolds number Re measured at different locations x downstream of the pipe inlet. The flow is continuously disturbed at the inlet. As the measurement location is moved downstream, the entire curve shifts to the left and steepens. Replotted from Rotta (1956).

turbulence at a given Re increases, and curves shift to the left. This illustrates that, even several hundred diameters downstream from the inlet, the flow has not settled to a steady condition. These long development lengths are the key difficulty in determining the true critical point and are caused by the excessive timescales that govern the dynamics in this regime, as discussed in Section 5.

2.4.2. Impulsive perturbations. More recent experiments employed impulsive perturbations (Wygnanski et al. 1975, Darbyshire & Mullin 1995), which are better suited for the study of transition. Such perturbations are typically realized by injection of a jet of fluid through one or multiple holes in the pipe wall. Single pulses can be used to initiate localized turbulent structures, and such experiments clarified the robustness of turbulent puffs as near equilibrium structures (Wygnanski et al. 1975), at least up the typical observation times in experiments.

Impulsive perturbations also allow the timing of the pulses to be adjusted, thereby providing an additional degree of freedom. Pulse length is crucial for determining the scaling of the turbulence transition threshold (Hof et al. 2003), whereas pulse frequency can be used to study the interaction between localized turbulent structures (Samanta et al. 2011). In particular, impulsive perturbations can trigger turbulence far more efficiently at low Re than their continuous counterparts. As shown in **Figure 4**, a continuous jet disturbance that locally causes very high fluctuation levels and a strong distortion of the flow profile fails to trigger puffs, and the downstream flow is fully laminar. An orifice inserted at the pipe inlet triggers puffs only sporadically and unpredictably, whereas an impulsive disturbance can trigger puffs in a controlled manner and with much lower overall disturbance amplitudes at the same Re. As argued by van Doorne & Westerweel (2009), puffs rely on the energy input from the impinging upstream laminar flow, and a sufficiently developed parabolic profile is required to keep the puff energetically sustained. Continuous perturbations distort the flow profile throughout, and, if they are of large amplitude, the resulting velocity profiles are too flat to sustain puffs. Counterintuitively, this causes flows to relaminarize (Kühnen et al. 2018). Likewise, if the spacing between two puffs is too small (less than $\sim 20D$), the downstream puff is exposed to the wake (i.e., the flat, energetically depleted profile) of the upstream puff and decays (Hof et al. 2010, Samanta et al. 2011). Hence, impulsive perturbations are a central tool for experimental studies because they can trigger single puffs in a controlled way down to low Re.

Once puffs are triggered, they lose any memory of their initiation (**Figure 4**). While close to the perturbation location the average flow structure depends on the perturbation type, at distances

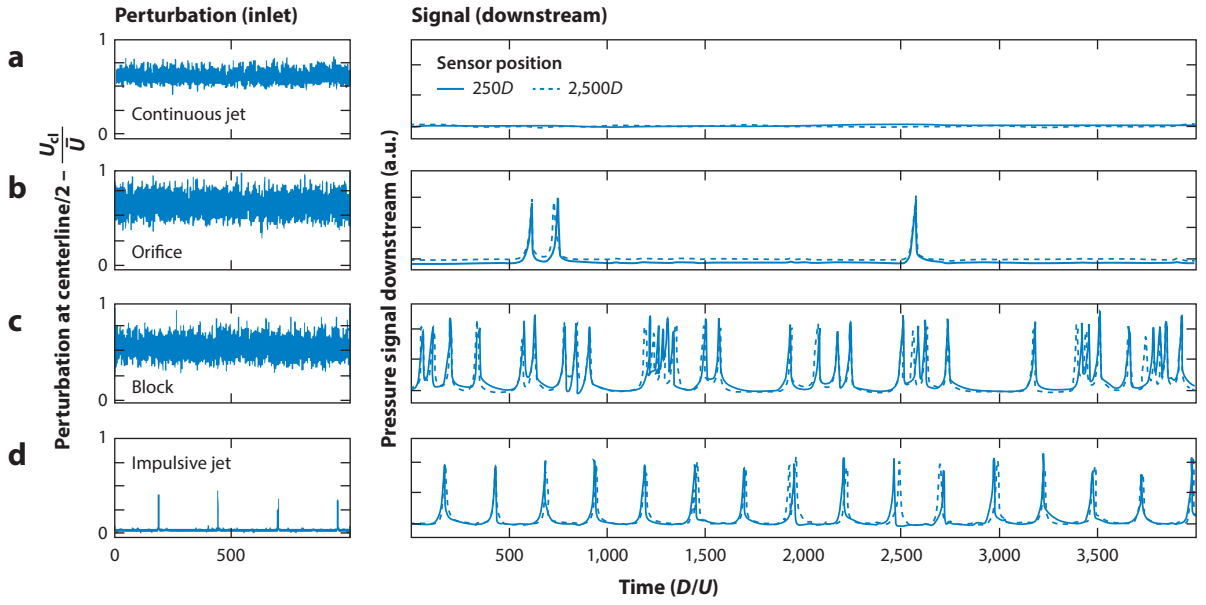

Figure 4

The left column shows the disturbance amplitude applied just downstream from the pipe inlet for four different perturbation types at Reynolds number $Re = 2{,}100$. The perturbation types are (*a*) continuous jets, (*b*) orifice, (*c*) partial blockage of the pipe, and (*d*) impulsive jets. The panels on the right show the corresponding pressure measurements at two downstream locations ($250D$ and $2{,}500D$). Spikes correspond to the passage of puffs. Figure adapted from Mukund & Hof (2018) with permission.

greater than $250D$ from the perturbation location, puffs are identical on average. This property also applies to injection perturbations that initially give rise to hairpin vortex streets (van Doorne 2004, Peixinho & Mullin 2007, Philip & Cohen 2010, Wu et al. 2015). While hairpin vortex structures can be triggered in the near wall region, as they progress further downstream either they decay and relaminarize or they develop into turbulence (van Doorne 2004), i.e., puffs or slugs, depending on *Re*.

3. INSTABILITY

We see from the above discussion how perturbations to laminar flow, whether natural or imposed, play an important role in experimental studies of pipe flow. This leads us naturally to our first perspective, also the oldest perspective, on the transition problem: that of hydrodynamic stability (**Figure 1*a***). We address the questions of which perturbations to laminar flow are most effective at triggering turbulence and how the required perturbation amplitude for transition depends on *Re*, i.e., how the threshold for transition depends on *Re* for a given perturbation type (**Figure 1*a***).

3.1. Linear Approaches to the Problem of Transition

The stability of laminar HP flow $\mathbf{U}_{\mathrm{HP}}$ to a perturbation $\mathbf{u}$ can be investigated by decomposing the full velocity field as $\mathbf{v} = \mathbf{U}_{\mathrm{HP}} + \mathbf{u}$, and inserting this into the incompressible Navier–Stokes equations, in dimensionless form

$$\frac{\partial \mathbf{u}}{\partial t} = -\nabla p + Re^{-1}\nabla^2\mathbf{u} - (\mathbf{U}_{\mathrm{HP}} \cdot \nabla)\mathbf{u} - (\mathbf{u} \cdot \nabla)\mathbf{U}_{\mathrm{HP}} - (\mathbf{u} \cdot \nabla)\mathbf{u}, \qquad 1a.$$

$$\nabla \cdot \mathbf{u} = 0, \qquad 1b.$$

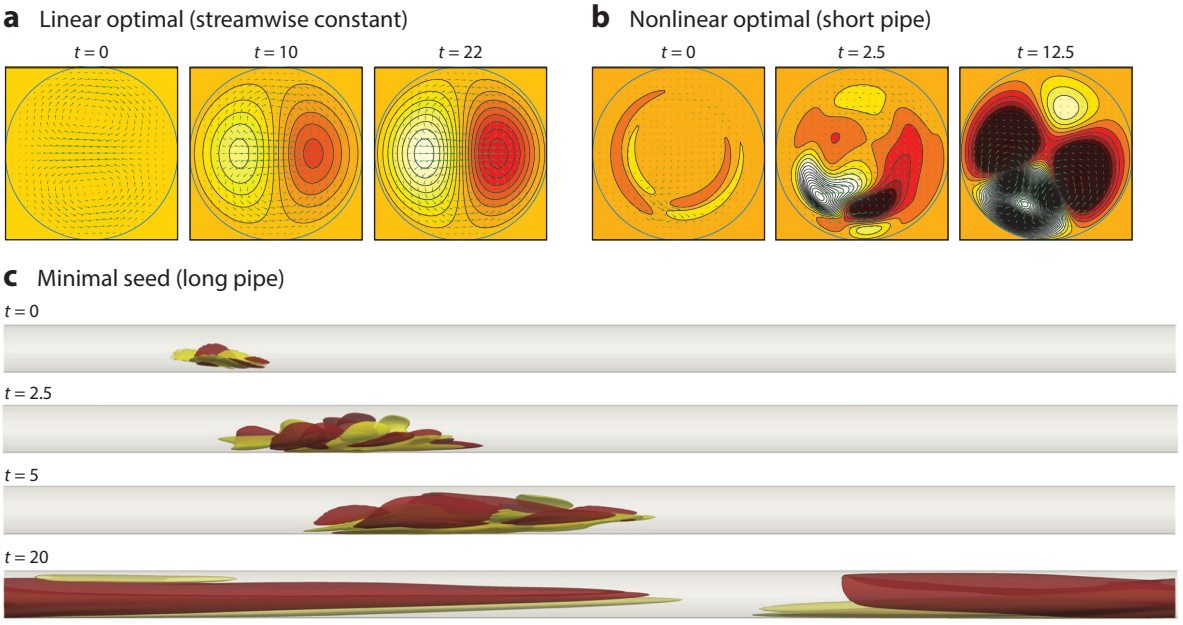

Figure 5

(*a*) Optimal linear nonmodal disturbance of pipe flow at Reynolds number $Re = 1{,}750$ consisting of a pair of streamwise vortices (*faint arrows*), which over time generates one streak of high streamwise velocity and one of low streamwise velocity. (*b*) Corresponding nonlinear optimal disturbance ($t = 0$) and its evolution for a pipe of length $L = (\pi/2)D$. In both panels, the color map runs from white and yellow, corresponding to low-velocity streaks, to red and black, corresponding to high-velocity streaks. Panels *a* and *b* adapted from Pringle & Kerswell (2010) with permission; copyright 2010 American Physical Society. (*c*) Snapshots of the temporal evolution of an initial condition close to the minimal seed at $Re = 2{,}400$ in a $25D$-long pipe. Panel *c* adapted from Kerswell (2018) with permission.

where p is the perturbation pressure (Drazin & Reid 2004). Even though Reynolds (1883) had stressed that "the condition might be one of instability for disturbance of a certain magnitude and stable for smaller disturbances," early theoretical approaches to the transition problem, led by luminaries such as Lord Rayleigh, Lord Kelvin, Lorentz, Orr, Sommerfeld, and Heisenberg, focused on the study of infinitesimal disturbances to laminar flow (Eckert 2010, 2015). This amounts to neglecting the last term in Equation 1a. Under the assumption of axial periodicity, the linear stability question reduces to a one-dimensional (radial) eigenvalue problem. Numerical solutions of this problem have determined that all eigenvalues have a negative real part, and hence HP is linearly stable, at least up to $Re = 10^7$ (Meseguer & Trefethen 2003).

Beyond $Re = 10^7$, it is difficult to keep disturbances at bay, even in double-precision calculations (Meseguer & Trefethen 2003). At the root of this behavior is the nonnormality of the linearized Navier–Stokes equations (Schmid & Henningson 2001, Schmid 2007). This situation arises because modal disturbances are not mutually orthogonal so that their linear combinations can give rise to large transient growth of nonmodal (shape-changing) disturbances, as first shown by Boberg & Brosa (1988) and later popularized by Trefethen et al. (1993).

For laminar pipe flow, streamwise vortices are the optimal nonmodal disturbances—those maximizing transient energy growth. Specifically, a streamwise vortex pair of infinitesimal amplitude ϵ lifts low-velocity fluid near the wall to the center and high-velocity fluid near the center to the wall (Brandt 2014), as shown in **Figure 5*a***, thereby generating local streamwise velocity differences (streaks) of amplitude ϵRe (Schmid & Henningson 1994). The fact that an order ϵ perturbation can generate an order ϵRe response in the flow is generally consistent with the experimentally

Modal disturbance: an eigenmode of the Navier–Stokes equations linearized about the laminar flow. Modal disturbances (or modes) do not change in shape as they grow or decay exponentially in time

Nonmodal disturbance: a superposition of eigenmodes. Nonmodal disturbances change shape as they evolve and can be transiently amplified before ultimately growing or decaying exponentially

determined transition threshold scaling as Re^{-1} for push–pull disturbances generating streamwise vortices in pipe (Hof et al. 2003, Mellibovsky & Meseguer 2007) and channel (Lemoult et al. 2012) flows.

Minimal seed: a disturbance of the least amplitude capable of triggering turbulence

While the linear transient growth of nonmodal disturbances is an essential feature of pipe flow, the linear picture is overly simplified (Waleffe 1995). Nothing guarantees that optimal linear disturbances will trigger turbulence in a fully nonlinear setting, and even if they do, there may be other disturbance types that are more effective. Sections 3.2 and 3.3 address the role of nonlinearity in the instability problem.

3.2. Streak Instability and Breakdown to Turbulence

An early approach to incorporating nonlinearity can be found in Boberg & Brosa (1988). When streamwise vortices are introduced at finite amplitude into the nonlinear Navier–Stokes equations (Equation 1), the strong streaks they generate can themselves become unstable, leading to turbulence. Studying the streak formation and breakdown process, Meseguer (2003) suggested that the threshold scaling was $Re^{-3/2}$, in agreement with the asymptotic analysis of Chapman (2002) for channel flow. Later, Peixinho & Mullin (2007) showed experimentally that oblique disturbances are more efficient than streamwise vortices in triggering turbulence, in agreement with a previous numerical study of channel flow by Reddy et al. (1998). We note that most experiments and direct numerical simulations have been conducted for $Re \leq 10{,}000$, and as suggested by Chapman (2002), higher Re may be required to uncover the true asymptotic scaling.

3.3. Fully Nonlinear Approach: Minimal Seeds of Turbulence

A general approach to finding the minimum perturbation amplitude necessary to trigger turbulence is to solve an appropriate nonlinear optimization problem. The idea is simple in principle: optimize nonlinear growth over all possible initial conditions. However, there are substantial mathematical and computational challenges to this approach (Monokrousos et al. 2011). The interested reader is referred to Kerswell (2018) for a review of optimization techniques for computing the optimal routes to turbulence and to Luchini & Bottaro (2014) for general adjoint approaches, including flow stability and sensitivity of disturbances for complex geometries.

Pringle & Kerswell (2010) computed nonlinear optimal disturbances for pipe flow in short periodic pipes of length $L = (\pi/2)D$ and found that these disturbances exhibit substantially larger amplification than do their linear counterparts. As shown in **Figure 5*b***, nonlinear optimal disturbances are localized in the wall-normal and azimuthal directions, and as they evolve they expand and exploit the classical lift-up mechanism. In long pipes, the minimal seed is additionally localized in the streamwise direction with length about $7D$ (Pringle et al. 2015) (see **Figure 5*c***). In experiments, $7D$ corresponds to the pulse duration beyond which the perturbation amplitude levels off; i.e., for shorter pulse duration, significantly larger perturbations are needed to trigger turbulence (Hof et al. 2003).

This fully nonlinear approach enables a clear-cut, although computationally expensive, approach to the threshold-scaling problem. Duguet et al. (2013) tackled this problem in Couette flow for $Re \leq 3{,}000$. Extending the computations to higher Re, and to pipe flow, remains a challenge.

4. DYNAMICAL SYSTEMS

We see from the above discussion that when laminar pipe flow is disturbed at finite amplitude, the flow may relaminarize or may become turbulent, depending on the Re and on the details of the disturbance. This highly nonlinear behavior can be naturally rationalized via the mathematical

formalism of dynamical systems (**Figure 1*c***). Here we present this perspective on the transition problem, with special emphasis on pinpointing the mechanisms giving rise to the chaotic dynamics associated with turbulent flow.

4.1. The Phase Space of a Fluid Flow

Eberhard Hopf (1948) argued that, to understand turbulence transition conceptually, "it is useful to visualize the solutions in the phase space Ω of the problem." Here a phase state of the system corresponds to a full velocity field $\mathbf{v}(r, \theta, z) \in \Omega$ defined over the whole pipe volume and satisfying the boundary conditions and the continuity equation. A trajectory in phase space $\mathbf{v}(r, \theta, z, t) \in \Omega$ corresponds to the temporal evolution of the velocity field starting from an initial condition $\mathbf{v}(r, \theta, z, 0) = \mathbf{v}_0$. As in Section 3.1, the state of the system is defined relative to the laminar flow with the perturbation field, $\mathbf{u} = \mathbf{v} - \mathbf{U}_{\mathrm{HP}}$. We rewrite the Navier–Stokes equations (Equation 1) as a dynamical system of formally infinite dimension,

$$\frac{\partial \mathbf{u}}{\partial t} = \mathbf{f}_{Re}(\mathbf{u}), \qquad 2.$$

where $\mathbf{f}_{Re}$ represents the right-hand side of the momentum equation (Equation 1a), subject to the divergence-free constraint (Equation 1b). Viscous dissipation reduces the relevant long-term dynamics of the system to finitely many degrees of freedom (Hopf 1948). This is consistent with the fact that one can capture the dynamics of Equation 2 via direct numerical simulations using a finite number of grid points or spectral modes. Following discretization, Equation 2 becomes a finite (albeit large) system of ordinary differential equations, and the corresponding phase space is finite dimensional.

Laminar flow, $\mathbf{u} = 0$, is a steady state (equilibrium) of the dynamical system; i.e., $\mathbf{f}_{Re}(0) = 0$. Turbulence, which is also a solution of the equations for suitable values of Re, is associated with a more intricate set of the dynamical system, such as a chaotic attractor. The relationship between laminar and turbulent flow in phase space can be visualized in two-dimensional projections (Gibson et al. 2008), as exemplified in the cartoon of **Figure 6*a***. This phase-space picture captures that the laminar flow is stable to small disturbances (trajectories that start near laminar flow return to laminar flow) but is unstable to large disturbances of appropriate form (trajectories starting from appropriate places in phase space evolve to the chaotic attractor). Trajectories starting exactly on the laminar–turbulent boundary (the basin boundary in **Figure 6*a***) become neither laminar nor turbulent but evolve toward a saddle state (Itano & Toh 2001). Technically, the laminar–turbulent boundary is an invariant manifold (Guckenheimer & Holmes 2002).

The minimal seed is the lowest-energy state on the laminar–turbulent boundary. Trajectories starting near the minimal seed evolve first toward the saddle state before being repelled toward laminar flow or turbulence, depending on which side of the boundary they start (Kerswell 2018). The actual phase-space relationship between laminar flow and turbulence is more nuanced (see **Figure 6*b***, which is discussed in Section 4.3).

4.2. Exact Coherent States and the Onset of Chaos

The onset of turbulence with increasing Re can be formulated in terms of the qualitative changes in phase space (or bifurcations) as a parameter is varied. At low Re, $Re < 81.49$, the system is highly dissipative, and all perturbations to laminar flow decay monotonically (Joseph & Carmi 1969). At higher Re, $Re \gtrsim 1{,}500$, turbulence can be observed in experiments (Hof et al. 2005), indicating the existence of invariant sets that are dynamically disconnected from laminar flow and support chaotic dynamics.

Chaotic attractor: an attracting invariant set exhibiting unpredictable but deterministic dynamics. Trajectories starting arbitrarily close on a chaotic attractor diverge from one another exponentially in time

Bifurcation: a qualitative change in the phase space of a dynamical system; occurs when a parameter crosses a critical point. At a bifurcation, the number, type, and/or stability of invariant sets changes

Invariant set: a set of states that is unchanged by temporal evolution. The simplest invariant sets are steady states and periodic orbits

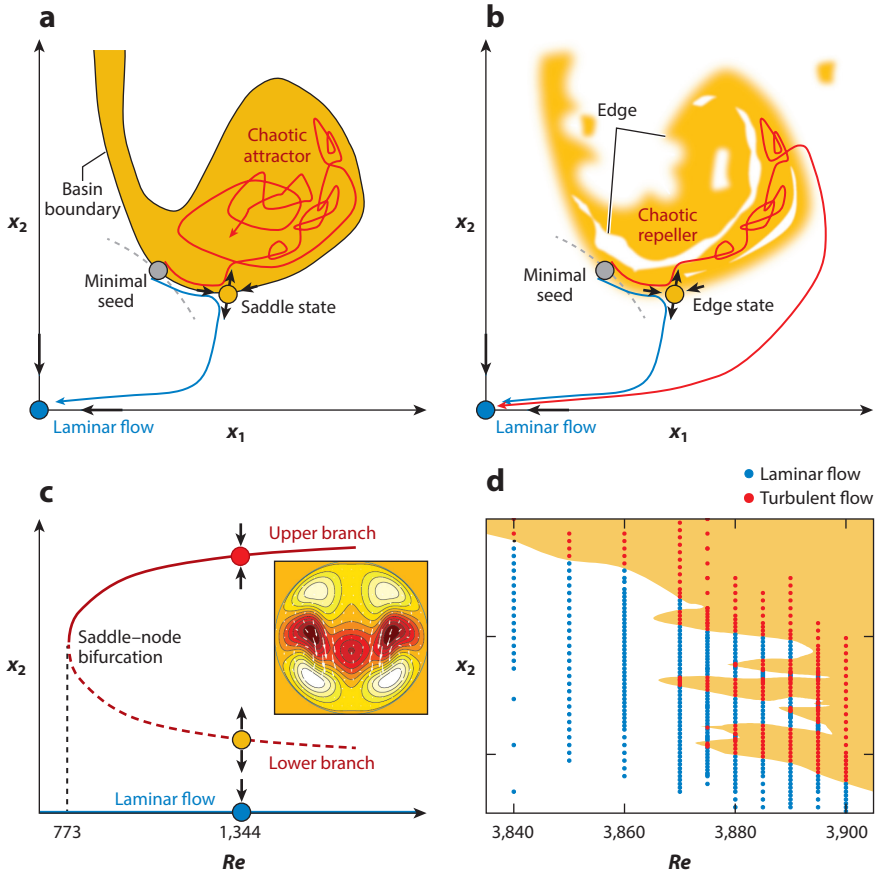

Figure 6

(*a*) Phase-space cartoon of a system in which a chaotic attractor (turbulence) and a steady state (the laminar flow) coexist. The basins of attraction of turbulence (*orange*) and of the laminar flow (*white*) are separated by the basin boundary. Trajectories starting near the minimal seed approach a saddle state before being repelled toward the chaotic attractor (*red* trajectory) or toward the laminar flow (*blue* trajectory). (*b*) As in panel *a*, but for a system in which a chaotic saddle supports transient turbulence. Here an invariant manifold (the edge) separates transient trajectories with long lifetimes from those relaminarizing directly. (*c*) Saddle–node bifurcation diagram for mirror-symmetric traveling waves in pipe flow. The snapshot is from the upper branch solution at Reynolds number $Re = 1{,}344$. Panel *c* adapted from Pringle & Kerswell (2007) with permission; copyright 2007 American Physical Society. (*d*) Stability threshold of laminar pipe flow to a disturbance consisting of a pair of axially modulated streamwise vortices in a periodic domain of length $5D$. Points correspond to initial conditions that evolve toward laminar and turbulent flow, respectively. Panel *d* adapted from Schneider et al. (2007) with permission.

Exact coherent states (ECS): exact solutions of the Navier–Stokes equations with simple temporal dynamics, such as traveling waves and relative periodic orbits

The first, nontrivial invariant sets to be discovered for pipe flow are traveling-wave solutions (Faisst & Eckhardt 2003, Wedin & Kerswell 2004), whose velocity field satisfies $\mathbf{u}(r, \theta, z, t) = \mathbf{u}(r, \theta, z - ct, 0)$. In the frame comoving at their propagation speed c (specific to each wave), they are steady. These types of solutions are referred to as exact coherent states (ECS), because they are spatially coherent, dynamically simple, exact solutions of the Navier–Stokes equations. There have been experimental observations of flow states resembling traveling waves, indicating their presence, at least transiently, in turbulent pipe flow (Hof et al. 2004, De Lozar et al. 2012). As

reviewed by Kawahara et al. (2012) and Graham & Floryan (2021), ECS have been instrumental in understanding many aspects of wall-bounded turbulence.

To date, several families of traveling waves have been discovered and classified according to their spatial symmetries (Pringle et al. 2009). They appear in pairs via saddle–node bifurcations, and their existence has been traced as low as $Re = 773$ (Pringle & Kerswell 2007), as shown in **Figure 6*c***. This demonstrates that bifurcations, and hence qualitative changes in phase space, can and do occur well before turbulence can be excited in experiments. Another type of ECS, known as relative periodic solutions, are time periodic in a comoving frame (Duguet et al. 2008a, Willis et al. 2013).

Duguet et al. (2008b) showed that traveling waves are part of the laminar–turbulent boundary for pipe flow. Moreover, if discrete spatial symmetries are imposed in the governing equations to restrain the dynamics, then the saddle state in the boundary is itself a traveling wave (Itano & Toh 2001, Duguet et al. 2008b). Some of these solutions are stable and can be computed by time-stepping the symmetry-restricted Navier–Stokes equations. This was exploited by Mellibovsky & Eckhardt (2012) to show how chaos emerges from a traveling wave via a sequence of bifurcations.

Saddle–node bifurcation: the birth of a pair of ECS at a critical saddle–node point. In the context of shear flows, the two branches of emerging solutions are termed the lower and the upper branch

Boundary crisis: a bifurcation in which simple solutions embedded in a chaotic attractor collide with its basin boundary (the edge), leading to a chaotic saddle

Chaotic saddle: a set in phase space supporting transient chaotic dynamics. Transients are characterized by a constant escape rate from the saddle, resulting in a memoryless relaminarization process

4.3. Boundary Crisis to Transient Chaos

The traveling waves and relative periodic orbits discussed in Section 4.2 have been obtained in short, axially periodic pipes and do not reflect the axial localization of turbulence occurring in puffs. The search for ECS in long pipes led to the discovery of spatially localized relative periodic orbits of pipe flow (Avila et al. 2013), shown in **Figure 7*a***. These ECS, their bifurcations, and their dynamics were computed in a symmetry subspace (twofold azimuthal periodicity and mirror symmetry) of the full Navier–Stokes equations. Unstable lower branch (LB) and stable upper branch (UB) states arise via a saddle–node bifurcation. The UB undergoes a sequence of bifurcations leading to chaotic dynamics (**Figure 7*b***). The chaotic attractor rapidly increases its volume in phase space, as seen in both the bifurcation diagram (**Figure 7*b***) and phase-space projection (**Figure 7*c***), until it touches the LB at a boundary crisis (Grebogi et al. 1982, Tél & Lai 2008). As a result, the phase space changes qualitatively (**Figure 6*b***): The basin boundary collapses, and the chaotic attractor turns into a chaotic saddle, or repeller. Trajectories starting within this region of phase space appear chaotic for some, potentially a long, time but eventually escape and go to the laminar state (the flow relaminarizes). The system is said to exhibit transient chaos. As **Figure 7*d*** shows, the escape process yields an exponential distribution of turbulent lifetimes. The mean lifetime of turbulence rapidly decreases as Re increases (Ritter et al. 2016). We stress that the transient dynamics in such symmetry-restricted simulations is far simpler than that of turbulent puffs in experiments. In the full unrestricted space, the dynamics is more complex, and lifetimes increase monotonically with Re (Brosa 1989, Faisst & Eckhardt 2004, Eckhardt et al. 2007). Uncovering the bifurcations leading to turbulent puffs remains an open challenge.

In systems with transient turbulence, the laminar–turbulent boundary is not a basin boundary but remains an invariant manifold, referred to as an edge (Skufca et al. 2006). In pipe flow, the edge has a fractal structure (Budanur et al. 2019). Regardless of how much one zooms into the chaotic saddle, initial conditions giving rise to long- and short-lived transients are found next to each other (Moehlis et al. 2004). The implication is that the stability threshold is a fractal hypersurface, as exemplified in **Figure 6*d***. For this reason, the threshold for the turbulent transition is shown as a region rather than a sharp curve (**Figure 1*a***). The relative attractor in the edge is referred to as an edge state and is chaotic in pipe flow (Schneider et al. 2007, Mellibovsky et al. 2009).

In summary, viewing the Navier–Stokes equations as a dynamical system provides valuable insights into the problem of transition, even in the absence of a linear instability of the laminar flow.

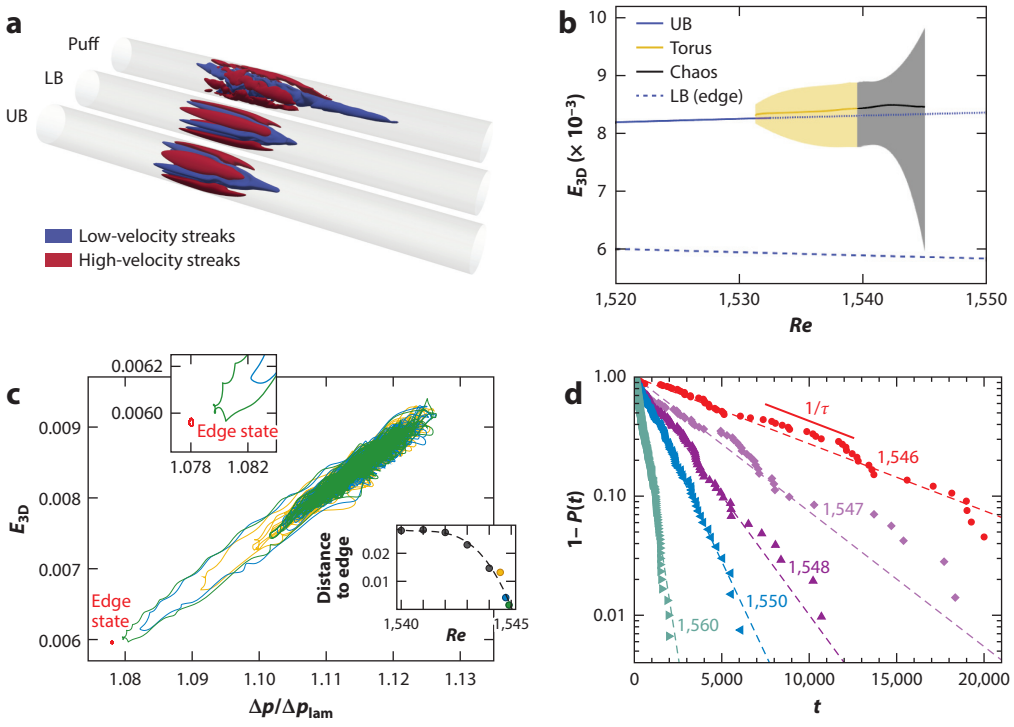

Figure 7

From spatially localized exact coherent states (ECS) to transient chaos in pipe flow. (*a*) Snapshots showing streaks of a turbulent puff, and lower branch (LB) and upper branch (UB) relative periodic orbits that emerge at a saddle–node bifurcation at Reynolds number $Re \approx 1{,}428$. Blue and red areas denote low- and high-velocity streaks, respectively. Panel *a* adapted from Avila et al. (2013) with permission; copyright 2013 American Physical Society. (*b*) Bifurcation diagram of ECS leading to chaos and then a boundary crisis. (*c*) Phase-space projection of typical chaotic trajectories. The red cycle corresponds to the LB edge state, shown in more detail in the upper inset. The lower inset shows the minimum distance between the chaotic trajectories and the edge state, which vanishes at a boundary crisis, $Re_{bc} \approx 1{,}545$. (*d*) Probability of survival of chaotic trajectories obtained from the relaminarization times (*symbols*) collected from direct numerical simulations with different initial conditions. The mean lifetime scales as $\tau \propto (Re - Re_{bc})^{-1}$. Panels *b–d* adapted with permission from Ritter et al. (2016) (CC BY 4.0).

Unlike for flows with linear instabilities, such as Rayleigh–Bénard convection and Taylor–Couette flow driven by inner cylinder rotation, the bifurcations in pipe flow are necessarily disconnected from laminar flow, and the resulting chaotic dynamics is found to be transient. Similar scenarios have been found for plane Couette flow (Kreilos & Eckhardt 2012, Lustro et al. 2019), for channel flow (Zammert & Eckhardt 2015), and even for magnetohydrodynamic Keplerian flows (Riols et al. 2013), suggesting that the emergence of transient chaos from ECS is generic in shear flows.

5. STATISTICAL PHASE TRANSITION

We see from the above discussion how linear and nonlinear methods can elucidate laminar flow's receptivity to perturbations, and we discuss above the insights that dynamical systems can provide regarding the origins of ECS and transient chaos. However, none of these perspectives can resolve what are probably the most intriguing aspects of the onset of turbulence in a pipe: the determination of a precise critical point as proposed by Reynolds and the associated universal nature of the transition to turbulence. The key difference with criticality in classic problems such as Taylor–Couette flow and Rayleigh–Bénard convection is that here we are concerned not with

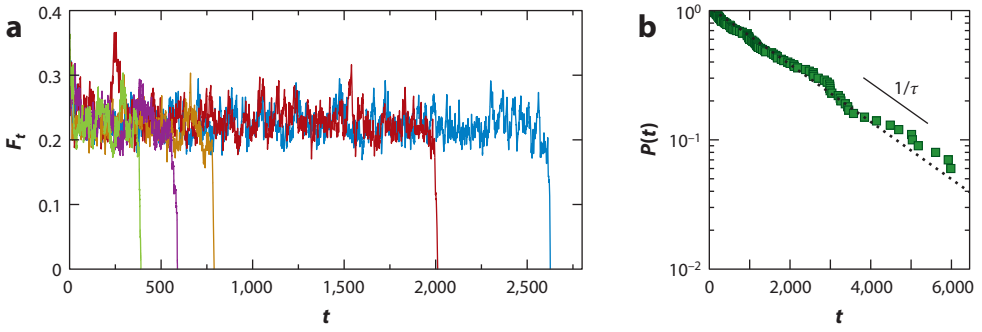

Figure 8

(*a*) Transient dynamics of turbulent puffs at Reynolds number $Re = 1{,}900$. Shown is the temporal evolution of turbulent fraction F_t from five direct numerical simulations of single puffs in a pipe of length $50D$. Each simulation is initialized with a different instantaneous snapshot of a turbulent puff at $Re = 2{,}200$. Puffs may persist for a significant time before abruptly decaying to laminar flow. (*b*) Probability of puff survival at $Re = 1{,}900$ collected from 100 independent simulations of single puffs such as those shown in panel *a*. Figure courtesy of Daniel Morón.

an upper stability limit of laminar flow, but instead with the lower stability border of sustained turbulence. While the former problems can be understood in terms of stability analysis and bifurcation theory, the latter is a direct transition to a fluctuating, spatially intermittent mixture of turbulent and laminar flow that is most appropriately characterized as a nonequilibrium statistical phase transition.

Most of the remainder of this review is devoted to understanding the dynamics of turbulence in both space and time. In this section we address how intermittent turbulence becomes sustained at a critical point, and in Section 6 we explain how localized turbulent puffs give way to expanding slugs.

5.1. Transient Turbulence

In Section 2.3, we show that at the lowest *Re* for which turbulence can be observed, it appears only in the form of localized puffs. Classical experiments led to the belief that puffs are themselves sustained turbulent structures, as highlighted by Wygnanski et al. (1975), who coined the term equilibrium puff. However, turbulent puffs are not sustained indefinitely. It has been experimentally (Peixinho & Mullin 2006, Hof et al. 2006) and numerically (Willis & Kerswell 2007) established that, at a fixed *Re*, different realizations of turbulent puffs will survive for different lengths of time before abruptly decaying to laminar flow, as illustrated in **Figure 8**. This is a prototypical example of metastability: Puffs appear to be stable equilibrium structures for a significant time before abruptly transitioning to a more stable state, in this case laminar flow. One refers to such abrupt relaminarization as puff decay. The statistics of the survival times from many realizations consistently give exponential distributions, as seen in **Figure 8**. Such distributions correspond to a constant probability per unit time for decay to occur, independently of the history of the puff. Hence, turbulent puffs do not age, and puff decay is effectively a memoryless (Poisson) process. The exponential distribution of survival times is consistent with a chaotic saddle in phase space. We see this in **Figure 7**, in which a chaotic saddle arises via a boundary crisis.

While the lifetime of any individual puff in simulation or experiment is not very meaningful, the mean lifetime of an ensemble of puffs at a fixed *Re* is, so much so that mean lifetimes are perhaps the most prevalent measurements made on puffs and one of the most useful quantities

Equilibrium puff: a historical term referring to a localized patch of turbulence that maintains nearly constant form and speed as it moves down the pipe. Equilibrium is a misnomer since puffs are metastable

Metastable state: a state that appears to be a stable equilibrium but that has a finite lifetime and eventually transitions to a more favored state. Puffs are metastable states

Puff decay: the abrupt relaminarization of a (metastable) turbulent puff. Puff decay results in a decrease in the turbulent fraction of the flow

available to characterize puffs at a given *Re*. Clearly, the statistical behavior of an ensemble of states is key to understanding the dynamics of turbulence near onset.

Studies of puff lifetimes in experiments (Peixinho & Mullin 2006) and direct numerical simulations (Willis & Kerswell 2007) suggested that the mean lifetime becomes infinite at a critical *Re*, beyond which the puffs would be truly stable (equilibrium) states. Within the dynamical systems perspective, this would correspond to the chaotic saddle (transient turbulence) transforming into a chaotic attractor (sustained turbulence) at a crisis bifurcation, or possibly via some other mechanism. However, experiments in a longer pipe and with better resolved statistics (Hof et al. 2006) revealed that puffs do not stabilize but remain transient. Their mean lifetimes were subsequently observed to grow faster than exponentially with *Re* (Hof et al. 2008) but nevertheless to remain finite for any *Re*. Hence, individual puffs never stabilize, and it is impossible to define a critical point from the perspective of individual puffs.

The faster-than-exponential, or superexponential, increase in mean lifetimes with *Re* was confirmed in direct numerical simulations (Avila et al. 2010) as well as in independent experiments (Kuik et al. 2010). Combined results from these studies are shown on the left branch of **Figure 9*a***, together with a double exponential fit to the dependence of mean lifetime on *Re*: $\tau = \exp[\exp(aRe + b)]$. Goldenfeld et al. (2010) proposed a simple mechanism connecting the superexponential scaling of lifetimes to extreme value distributions. Nemoto & Alexakis (2021) refined the details of this mechanism on the basis of extreme values of vorticity from direct numerical simulations of turbulent puffs. More generally, transient turbulence has been observed for a range of different shear flows and is one of the best established properties of transitional turbulence. The extreme dependence of lifetimes on *Re* makes lifetime measurements ideally suited to calibrate different experiments and to quantitatively compare experiments to simulations.

5.2. The Critical Point

The quest for a critical point cannot be resolved by considering the decay of puffs alone. The mechanism by which turbulence becomes sustained is more complex. A particularly insightful theoretical approach was introduced by Kaneko (1985), who developed a new paradigm by enlarging the dynamical systems framework to spatially extended systems. He considered turbulence to be a product state of multiple chaotic systems coupled in physical space and showed that locally transient chaos can become sustained through spatial coupling. Specifically, Kaneko studied coupled one-dimensional maps on a discrete spatial lattice (coupled map lattice). In the absence of spatial coupling, the dynamics at each lattice site is transient chaos, with eventual decay to a steady laminar state. With nearest-neighbor coupling, the spatially extended system does not necessarily decay to the laminar state. Instead, it can reach a persistent state composed of a mixture of chaotic and laminar sites varying in space and time. Kaneko referred to these dynamics as spatiotemporal intermittency.

Coming from a different perspective, Pomeau (1986) also recognized the importance of approaching subcritical transition as a spatiotemporal problem, and he proposed a connection to a nonequilibrium statistical phase transition known as directed percolation (DP) (see Hinrichsen 2000 and Lübeck 2004 for extensive reviews of nonequilibrium phase transitions, with emphasis on DP in particular). We address this phase transition after presenting further phenomenology for pipe flow. However, very much like the Kaneko picture, the essential point is to consider transition in large spatially extended systems in which turbulence and laminar flow coexist in different spatial regions, evolving in space and time in a complex (intermittent) way.

The first studies of subcritical transition from a spatiotemporal perspective were for plane Couette flow (Bottin & Chaté 1998, Bottin et al. 1998; see the review by Manneville 2015). For pipe flow, Moxey & Barkley (2010) noted the significance of the spatiotemporal framework to

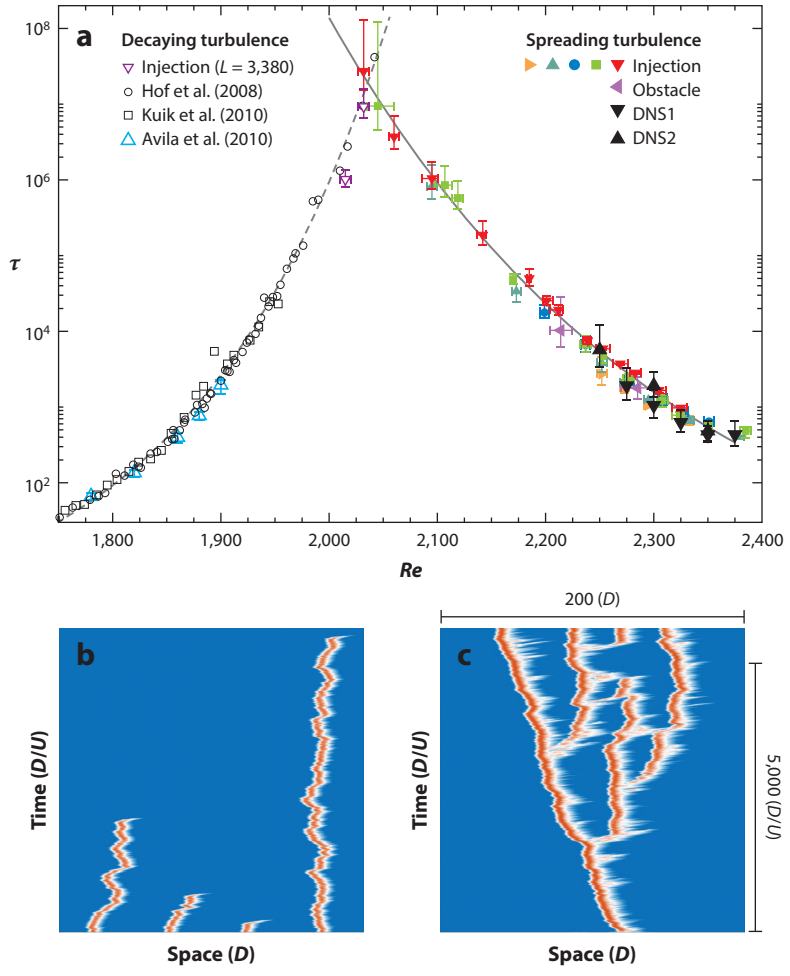

Figure 9

(*a*) Mean lifetime of a puff before a decay or splitting event. The left branch shows mean lifetimes for puff decay from experiments and numerical simulations. The dashed curve is given by $\tau = \exp[\exp(0.005556Re - 8.499)]$ and approximates the Reynolds number Re dependence of the mean lifetime for decay. The right branch shows mean lifetimes for a puff splitting event. The solid curve is given by $\tau = \exp[\exp(-0.003115Re + 9.161)]$ and approximates the Re dependence of mean time until a daughter puff is nucleated and the turbulent fraction increases. Both curves represent superexponential scaling with Re and cross at $Re = 2{,}040 \pm 10$. Panel adapted from Avila et al. (2011) with permission. (*b*,*c*) Spatiotemporal visualizations of puffs below ($Re = 1{,}900$) and above ($Re = 2{,}300$) the critical point. Visualizations are in frames of reference moving with the average puff speed and the center of mass of the intermittent region, respectively. In panel *b*, the flow is initiated with several puffs, which subsequently decay, resulting in laminar flow (the absorbing state). In panel *c*, the flow is initiated with a single puff that splits, creating daughter puffs and leading to an intermittent mixture of turbulent and laminar flow. Panels *b* and *c* provided by Daniel Morón.

the observed irregular (intermittent) occurrence of multiple puffs in long pipes. In particular, they pointed out that puff splitting (Lindgren 1957, Wygnanski et al. 1975, Shimizu et al. 2014) provides the proliferation mechanism for turbulence to become sustained, despite the transient nature of individual puffs. **Figure 9*c*** illustrates puff splitting in a numerical simulation of pipe flow. The flow is initiated with a single puff that subsequently generates additional daughter puffs, thereby increasing the turbulence fraction of the flow.

Avila et al. (2011) noted that puff splitting is a memoryless process that, like puff decay, can be quantified in terms of a mean time: the average time for a puff to undergo a first splitting. Mean splitting times were measured as a function of *Re* and were also found to scale superexponentially with *Re*, indicating that there is no value of *Re* where the mean splitting time becomes infinite. **Figure 9*a*** shows the measured mean times for decay and splitting. The *Re* dependence of the decay and splitting statistics approximately mirror one another such that curves cross at a critical *Re*, estimated to be $Re = 2{,}040 \pm 10$. At this critical value, the two timescales are balanced. Below the crossing, puff decay will dominate puff proliferation (**Figure 9*b***), while above the crossing, proliferation will dominate decay (**Figure 9*c***).

Puff splitting: the generation of a second daughter puff on the downstream side of a (metastable) puff. Puff splitting results in an increase in the turbulence fraction of the flow

Absorbing state: in nonequilibrium statistical phase transitions, an absorbing state is a state that, once reached, cannot be left spontaneously. Laminar Hagen–Poiseuille flow is the absorbing state for pipe flow

Turbulent fraction F_t: the fraction of space, at a fixed time, occupied by turbulent flow

At the critical point defined by the crossing of mean lifetimes, the common mean timescale for a puff to either split or decay is $\sim 2 \times 10^7$ advective time units. This corresponds to a puff traveling on average a distance of $\sim 2 \times 10^7$ pipe diameters before it either splits or decays. These enormous timescales and space scales explain why earlier studies, such as the study by Rotta (1956) shown in **Figure 3**, could not have converged on a critical point. To determine the critical point directly using Reynolds' approach (see the sidebar titled Reynolds Critical Point), one needs to trigger turbulence and let it evolve over extraordinarily long distances to determine whether the turbulence is sustained. This approach would seem to rule out studying the full spatiotemporal problem with many interacting puffs near the critical point. However, Mukund & Hof (2018) exploited the memoryless nature of puffs to design an experimental pipe with effectively periodic boundary conditions by having it trigger a new puff at the entrance every time a puff exited the pipe downstream.

The balance between decay and splitting timescales of isolated puffs is a simplification of the full process by which turbulence becomes sustained, since it ignores the puff interactions that will necessarily occur after splitting takes place. This is evident in **Figure 9*c***, in which one can observe a puff terminating due to interaction with a neighboring puff. Mukund & Hof (2018) demonstrated that, at $Re = 2{,}060$, intermittent flow with many turbulent puffs eventually settles into a statistically steady-state (requiring measurement times of $\sim 6 \times 10^7$ advective time units) decay. At $Re = 2{,}020$, and hence slightly below the critical point, all puffs eventually decay (after $\sim 10^8$ advective time units).

With these observations in mind, we return to nonequilibrium statistical phase transitions and to DP in particular. **Figure 9*b*** illustrates the eventual decay of multiple puffs. At the end of the simulation, the flow is everywhere in the laminar state, referred to as an absorbing state in statistical physics. The active state, turbulence, can never spontaneously emerge from the absorbing state because laminar flow is linearly stable. It can arise only via local proliferation from existing turbulence. Turbulence is a fluctuating state with statistical probabilities of decaying and proliferating, and the ratio of these probabilities depends on a control parameter, *Re*. These are the key ingredients of DP. The percolation is directed because time is not reversible; turbulence is clearly percolating upward in time in **Figure 9*c***.

The following features can be expected if pipe flow exhibits a statistical phase transition of DP type. There will be a critical *Re* below which the flow will always eventually reach the absorbing state from any turbulent initial condition. Above the critical *Re*, the flow, if initiated with turbulence, will eventually reach a statistical equilibrium with an average turbulence fraction, F_t, that depends only on *Re*. This equilibrium value of F_t will grow continuously from zero at the critical *Re* (shown schematically in **Figure 1*b***). Finally, there will be universal scaling laws (critical exponents) associated with the transition (see Hinrichsen 2000, Lübeck 2004).

Pipe flow appears to have all the necessary ingredients for the transition to turbulence to be in the DP universality class. The laminar HP flow is linearly stable and is hence an absorbing state in the context of DP. Indeed, the transitions to turbulence in axially confined (Lemoult et al. 2016)

and unconfined (Klotz et al. 2022) circular Couette flow as well as planar Waleffe flow (Chantry et al. 2017) have all been shown to fall into the DP universality class. For pipe flow, experimental observations by Mukund & Hof (2018) show that at $Re = 2{,}020$ an initially turbulent flow eventually reaches the absorbing state, while at $Re = 2{,}060$ a very low persistent F_t is attained. These observations suggest that the transition is probably continuous. Furthermore, model studies by Barkley (2011, 2016) and Shih et al. (2016) support the continuous nature of the transition and suggest that it falls into the DP universality class. However, currently there is no direct measurement from either direct numerical simulations or experiments confirming that F_t grows continuously from zero or that the transition belongs to the DP universality class. Establishing either of these as fact remains one of the great challenges for pipe flow.

Directed percolation (DP) universality class: a class of nonequilibrium phase transition characterized by a specific set of critical exponents. If a system displays scaling with these exponents, it is said to be in the DP universality class

Weak and strong slugs: turbulent slugs with weak and strong downstream fronts, respectively

Weak front: a turbulent–laminar front where turbulence decays monotonically to laminar flow

Strong front: a turbulent–laminar front where turbulence is produced, with an associated spike in the turbulent kinetic energy

6. PUFF–SLUG TRANSITION

Above we discuss the fundamental role that localized turbulence puffs play in the onset of sustained turbulence. At a higher *Re*, the situation changes fundamentally, and once triggered, turbulence aggressively expands at the expense of laminar flow in the form of slugs (recall Section 2.3 and **Figure 2**). Intermittency is ultimately lost, leading to fully turbulent pipe flow. Only after turbulence becomes statistically uniform in the axial direction does the flow obey the Blasius friction law (Avila & Hof 2013). In this section, we address the transition from puffs to slugs.

Figure 10 illustrates the scenario by which turbulence changes from localized puffs to expanding slugs. Panels *b–d* of **Figure 10** show the evolution from localized patches of turbulence at three different *Re*. At lower values of *Re*, turbulence remains in localized puff form, while at higher values of *Re*, turbulence rapidly expands. The frame of reference is that of the bulk velocity, so structures moving to the left propagate upstream relative to the bulk velocity, while structures moving to the right propagate faster than the bulk velocity. There are two distinct types of slugs: weak and strong (Barkley et al. 2015). These are distinguished by their downstream turbulent–laminar fronts, as we explain in more detail below. While the puff shown in **Figure 10*b*** eventually undergoes decay or splitting, those timescales are extremely long in comparison with the relevant timescales considered here. **Figure 10*a*** shows upstream and downstream front speeds of the turbulent patches as a function of *Re* for both pipe flow and square duct flow.

Early measurements of the onset of expanding turbulent slugs can be found in Lindgren (1957). Lindgren associated a critical *Re*, R_K, with the transition to expanding turbulence and notes that for $Re < R_K$ turbulence existed only as "flashes" of "unaltered length," whereas above this value turbulence "elongates itself continually." The significance of the transition to slugs and the role of turbulent–laminar fronts were recognized by Coles (1962), who summarized important aspects of early experiments by Rotta (1956), Lindgren (1957), and himself (unpublished). Turbulent slugs have since been the subject of numerous experimental and numerical studies (Lindgren 1969, Wygnanski & Champagne 1973, Darbyshire & Mullin 1995, Durst & Ünsal 2006, Nishi et al. 2008, Duguet et al. 2010, Song et al. 2017, Rinaldi et al. 2019). Chen et al. (2022) recently studied slugs numerically up to $Re = 10^5$ and compared their results with several of these previous studies. Upstream front speeds are reasonably consistent across multiple studies. Downstream front speeds have proven more difficult to obtain consistently, particularly above $Re = 10^4$. Chen et al. (2022) find, from their data, high-*Re* scaling laws for upstream and downstream front speeds of the form $c_{up} \simeq 0.024 + (Re/1{,}936)^{-0.528}$ and $c_{down} \simeq 1.971 - (Re/1{,}925)^{-0.825}$.

6.1. Physical Mechanisms

Figure 11 explains the physical mechanism underlying the transition from localized to expanding turbulence. Shown are turbulent kinetic energy (TKE) budgets for a puff and the two types

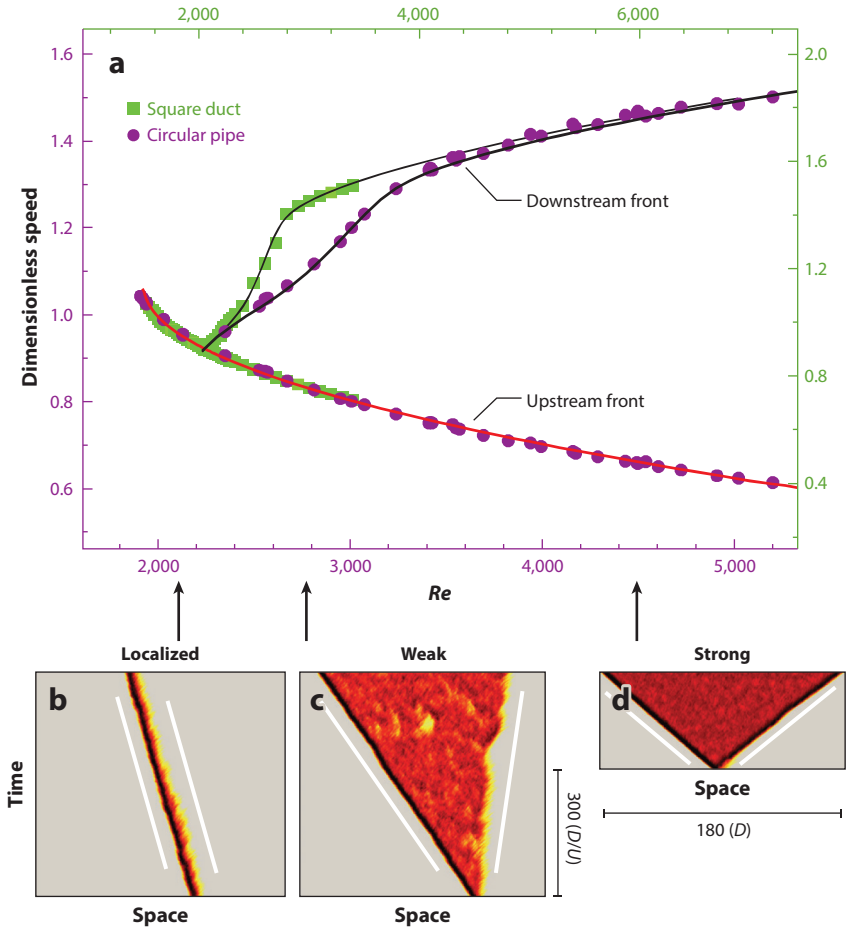

Figure 10

Puff-to-slug transition. (*a*) Upstream and downstream front speeds as a function of Reynolds number *Re* for pipe flow and square duct flow. Points are from experiments and direct numerical simulations. The difference between the upstream and downstream speeds quantifies the rate of expansion of slug expansion. (*b–d*) Space–time visualizations from direct numerical simulation of pipe flow showing a localized puff and expanding slugs in a frame of reference moving at the bulk velocity. In this reference frame, upstream (*left*) fronts are seen to move upstream. The two types of slugs, weak and strong, are distinguished by their downstream (*right*) fronts. The curves in panel *a* represent speeds obtained from a model that captures the details of the transition from localized puffs to weak slugs to strong slugs. Figure adapted from Barkley et al. (2015) with permission.

of slugs (Song et al. 2017). It is instructive to consider first the strong slug (bottom panels of **Figure 11**). At the intense upstream front, production exceeds dissipation, and there is a net production of TKE. Since this front is moving upstream relative to the mean flow, upstream fluid crosses the front. Essentially, the kinetic energy contained within the laminar upstream flow is fuel for this front. The front burns this fuel, converting laminar kinetic energy into TKE. At a short distance downstream from the production maximum, production and dissipation of TKE come into balance, $P = \epsilon$, and form the core of the slug—or what is termed turbulent pipe flow once turbulence fully occupies the pipe.

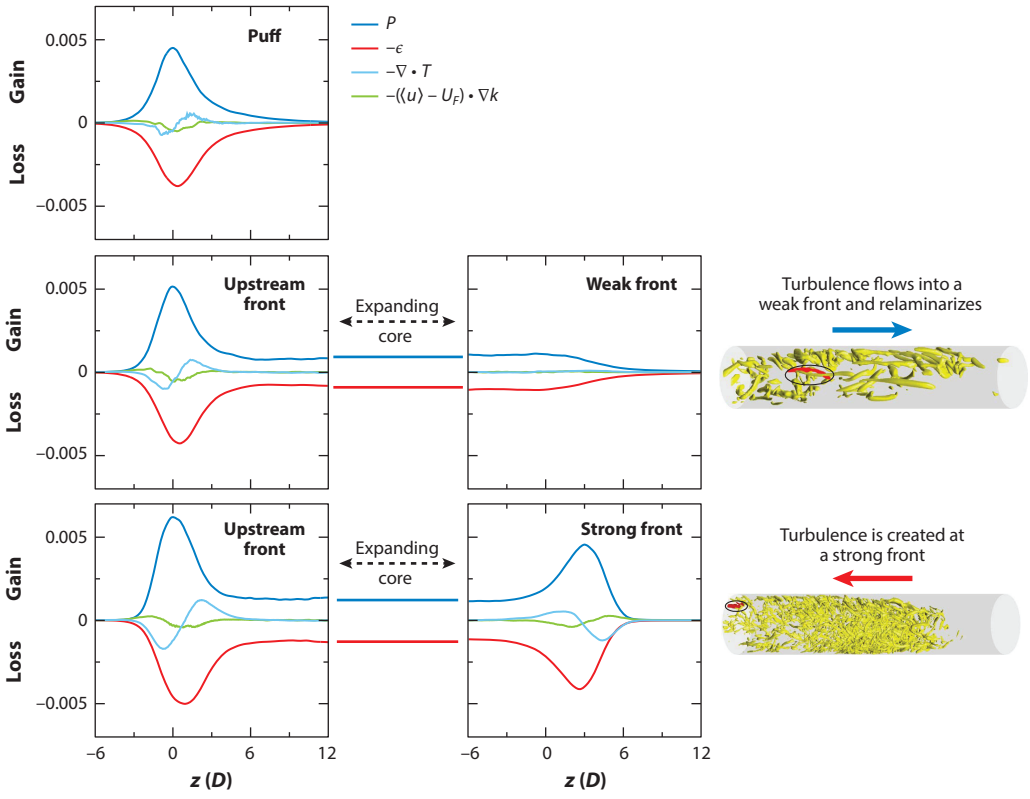

Figure 11

Turbulent kinetic energy budgets for puffs and slugs. Budgets are obtained in frames of reference in which the structures are stationary, and hence the budgets are in different reference frames for the upstream and downstream slug fronts. The most significant contributions are from production P and dissipation ϵ, which come into balance in the core region of the slugs. Turbulence moves into a weak downstream front, where it relaminarizes. Turbulence is generated at a strong downstream front and, relative to the front, moves into the core of the slug. Top panel adapted from Song et al. (2017) with permission, with additional data in the top panel provided by Baofang Song.

The downstream turbulent–laminar front of the strong slug is similar to a reflection of the upstream front. This front overtakes the laminar flow downstream, and there is also net production of TKE at the front. In the frame of reference of the front, laminar downstream fluid crosses into the front, wherein turbulence is produced and flows into the core of the slug as it expands. Hence, there is an increase in the total TKE of the flow coming from both the upstream and downstream fronts.

The downstream turbulent–laminar front of the weak slug is different. Seen in the reference frame of the front, turbulence from the core of the slug flows into the front, where it decays (relaminarizes). Weak slugs effectively contract at their downstream front. There is nevertheless an overall expansion of these slugs due to the speed difference between the upstream and downstream fronts. The increase in the total TKE associated with expansion comes from the net production at the upstream front only.

To understand the puff, consider what happens to the slug as the Re is decreased, i.e., viscosity is increased. There comes a point at which TKE production in the core of the slug can no longer balance the increased dissipation due to the increase in viscosity. The core collapses. However, at the upstream front, production is still large, and so it survives the increase in viscosity. The upstream front and the weak downstream front coalesce and become the puff: an isolated

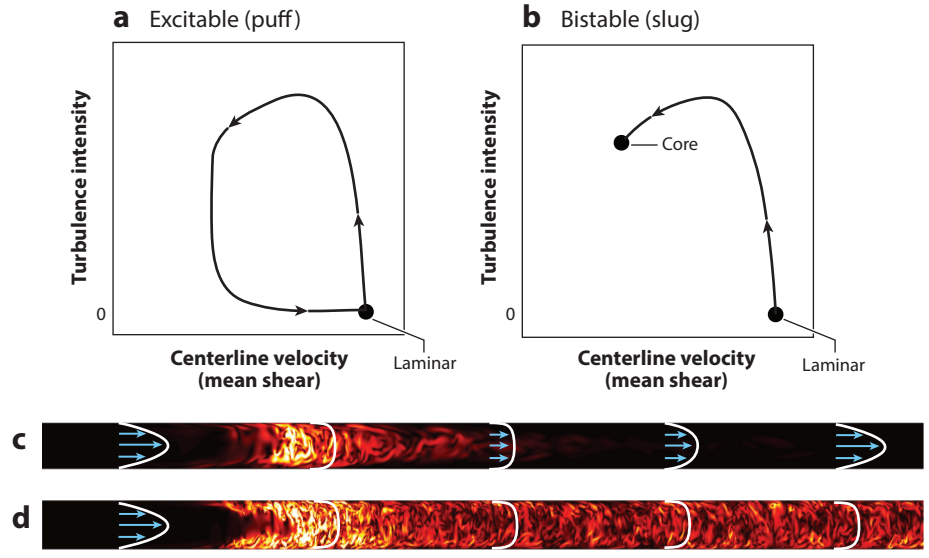

Figure 12

The puff-to-slug transition as a transition from excitability to bistability. (*a*,*b*) Phase planes of centerline velocity (equivalently the mean shear) and turbulence intensity. Trajectories illustrate the evolution of these quantities as a function of position along the pipe, with arrows indicating increasing downstream location. The trajectories shown are schematics only. Examples from simulations can be found in Song et al. (2017) and Rinaldi et al. (2019). (The phase planes represent quantities different from those in **Figure 6**.) (*c*,*d*) Visualization of a puff and the upstream front of a slug. Turbulent fluctuations from numerical simulations are shown in color. White curves are schematic representations of the mean velocity profiles at various axial locations. Numerical simulations provided by Baofang Song.

structure continually burning upstream laminar kinetic energy but leaving no persistent downstream turbulent slug. The continuous variation of the upstream front speeds throughout the transition from puffs to slugs in **Figure 10** is a direct reflection of the continuous evolution of the upstream fronts in **Figure 11**.

6.2. Excitability and Bistability

The transition from puffs to slugs is a transition from excitability to bistability (Barkley 2011, Barkley 2016; Barkley et al. 2015; Song et al. 2017). This transition, illustrated in **Figure 12**, is closely tied to the physical mechanisms just discussed. We focus on the interplay between turbulence and the mean velocity profile. Consider first the slug shown in **Figure 12*d*** and how the turbulence and profile evolve as a function of axial location, shown schematically as a trajectory in **Figure 12*b***. Upstream the flow is laminar: There is no turbulence, and the centerline velocity is high. Upon crossing the upstream front, there is a rapid increase in turbulence, which then causes the profile to blunt (the centerline velocity decreases). Downstream from the front, production and dissipation come into balance in the core of the slug. There are two stable states—laminar flow and the core of the turbulent slug—and the system is said to be bistable. The front connects these two stable states. Trajectories corresponding to downstream fronts of slugs are not shown but can be found in Barkley (2016), Barkley et al. (2015), and Song et al. (2017).

Now consider the puff in **Figure 12*c***. Just as for the slug, upstream from the puff, the flow is laminar, and crossing into the puff, there is a rapid increase in turbulence, causing the shear profile to blunt. Unlike for the slug, however, once the shear profile blunts, there is insufficient

production to balance dissipation. There is no stable state corresponding to the core of the slug. As a result, turbulence decays, after which the shear profile eventually recovers its parabolic form. The corresponding trajectory is illustrated in **Figure 12*a***. The system is said to be excitable.

The transition from excitability to bistability, coupled with downstream advection and fluctuations intrinsic to the turbulent state, can account for all the spatiotemporal phenomena presented in this review. Specifically, a simple model (Barkley et al. 2015) produces the front speeds shown as continuous curves in **Figure 10*a***. The same model also captures puff splitting and puff decay, the associated superexponential scaling of the mean lifetimes and a critical point at which the mean lifetimes cross, localized edge states, the interactions between puffs (puff pushing), and the laminar holes that can appear within turbulent flow. All of these phenomena are generic consequences of the transition from excitability to bistability in the presence of a fluctuating excited state. See Barkley (2016) for full details.

7. DIFFERENT GEOMETRIES AND ADDITIONAL CONTROL PARAMETERS

Pipe flow is a valuable prototype for the onset of turbulence in other wall-bounded shear flows, including linearly stable flows such as duct and plane Couette flow, as well as channels and boundary layers. In these flows, turbulence frequently sets in for *Re* lower than the linear instability of the laminar flow. These flows are often richer than pipe flow—e.g., many exhibit striped laminar–turbulent patterns near transition (Tuckerman et al. 2020)—but they nevertheless share common features with pipe flow, such as the coexistence of laminar and turbulent flow and the transient nature of turbulent patches. In ducts (Takeishi et al. 2015), Couette flow (Lemoult et al. 2016), and annular pipe flows (Ishida et al. 2016, 2017), the lateral aspect ratio of the system acts as an additional parameter, which allows for the unfolding of the dynamics from one dimensional (puffs) to two dimensional (spots or stripes). Significantly, in all these cases the laminar flow is linearly stable and is hence an absorbing state in the context of DP. This offers a possible unifying framework for the onset of sustained turbulence. Arguably, the subsequent transition to fully turbulent flow (the puff-to-slug transition) is far more important in practice. This latter transition is, however, not sharp and lacks universal properties such as critical exponents with which to make quantitative comparison between flows.

The understanding of transition in pipe flow has also allowed for the identification and demarcation of other instabilities and types of disordered motion that may arise in pipes when additional control parameters are introduced, for instance, in viscoelastic fluids, particle suspension, flows in curved pipes, or pulsatile flows. In each of these cases, a second control parameter appears in addition to *Re*. To understand how the transition to turbulence is affected by the second parameter, a number of recent studies have focused on puff lifetimes. Puff lifetimes are extremely sensitive to parameter changes and are therefore ideally suited to monitor the changes in the transition threshold as a control parameter is varied. For polymer drag reduction, by increasing polymer concentration (i.e., increasing viscoelasticity/Weissenberg number), the transition to ordinary turbulence is delayed (**Figure 13*a***). However, for sufficiently high concentrations a new instability (**Figure 13*a***) gives rise to the state of elastoinertial turbulence (Samanta et al. 2013). This flow state is characterized by lower fluctuation levels, the absence of hysteresis, and the lack of laminar–turbulent intermittency. The same strategy has been applied to pulsatile flows, where again turbulence is delayed and a instability to a helical mode arises with increasing pulsation amplitude (Xu et al. 2020). Likewise, in curved pipes the transition to turbulent puffs is postponed as the curvature increases (Sreenivasan & Strykowski 1983, Noorani et al. 2013, Kühnen et al. 2015) (**Figure 13*c***). Finally, in pipe flows of particle suspensions (Matas et al. 2003, Hogendoorn

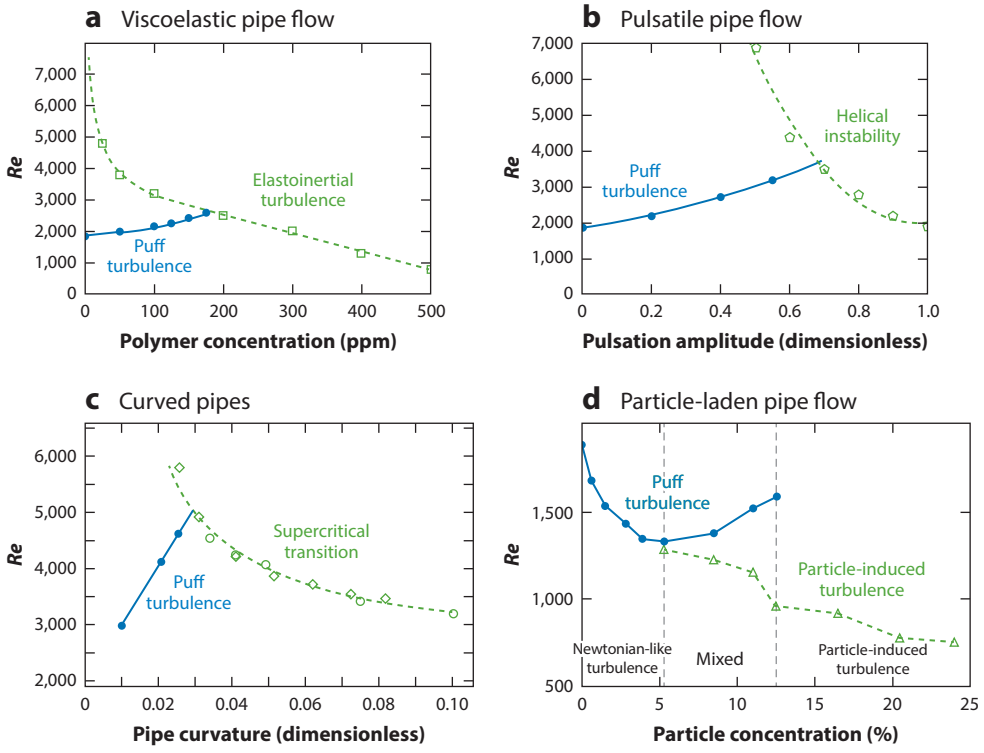

Figure 13

New instabilities that arise in pipe flows when additional control parameters are introduced. (*a*) The addition of long-chain polymers delays the puff transition (*blue*) and gives rise to an elastoinertial instability (*green*) and the associated state of elastoinertial turbulence. (*b*) Flow pulsation also delays the puff transition (*blue*), and increasing pulsation amplitudes give rise to (subcritical) helical instability (*green*). (*c*) Pipe curvature delays (Sreenivasan & Strykowski 1983) the puff transition (*blue*) and gives rise to a linear instability of the laminar Dean flow. (*d*) The addition of neutrally buoyant spherical particles pushes the puff transition to lower Reynolds numbers *Re* (Matas et al. 2003) and causes a new type of disordered motion (*green data points*). Panels adapted with permission from (*a*) Samanta et al. (2013), (*b*) Xu et al. (2020), (*c*) Kühnen et al. (2015), and (*d*) Agrawal et al. (2019).

& Poelma 2018, Agrawal et al. 2019), particle concentration leads to an early puff transition, but eventually another instability mechanism is encountered, featuring neither laminar–turbulent intermittency nor hysteresis (**Figure 13*d***). In conclusion, in more complex situations, different instabilities arise that eventually entirely suppress the transition scenario described above. Viewed in this multiple control parameter setting, the transition we describe in this review is hence only one out of several that can be encountered in pipe flows of complex fluids or more complex geometries.

8. SUMMARY AND SUGGESTIONS FOR FUTURE WORK

The turbulence problem associated with "wet water running through a pipe" is multifaceted. As we present here, there is not just one answer to the question of how transition occurs in pipe flow. To a significant degree, the question is in the eye of the beholder. The question may address the response of a laminar flow to a perturbation, it may address the continuous transition from turbulence back to laminar flow at the critical point, or it may refer to the process by which turbulence forms in a mathematical sense from simple invariant solutions to the Navier–Stokes equations.

As all of these are valid questions to ask, we review above the contributions that these various interconnected perspectives bring to our understanding of the transition to turbulence in a pipe.

SUMMARY POINTS

1. The threshold for transition from laminar flow to turbulence depends on perturbation type and amplitude. Nonlinear stability analysis determines the lowest-energy disturbance capable of triggering turbulence (the minimal seed) and hence the threshold scaling.
2. Dynamical systems approaches provide a conceptual framework for understanding the phase space of the Navier–Stokes equations. Bifurcation theory elucidates how new invariant sets come into existence as the Reynolds number Re is increased and provides insight into the origin of transient turbulence via a boundary crisis.
3. At low Re, turbulence exists in the form of localized puffs. These are transient states that, after a potentially very long time, abruptly revert to laminar flow (decay) or shed a daughter puff (puff splitting). Decay and splitting are memoryless processes characterized by their Re-dependent mean times.
4. Turbulence is first sustained indefinitely above the critical point $Re \approx 2{,}040$. This occurs once the mean splitting time is shorter than the mean decay time. Above the critical point, turbulence forms a complex spatiotemporal pattern.
5. At higher Re, localized turbulent puffs give way to expanding turbulent slugs, ultimately leading to space-filling turbulence. The transition from puffs to slugs is a transition from excitability to bistability.

FUTURE ISSUES

1. The practicality of dynamical systems approaches beyond transition is unclear. As Re increases, the number of exact coherent states (ECS) required to capture the dynamics of turbulence may grow explosively, and no general scheme has been devised so far to find dynamically relevant ECS. New methods, e.g., those based on machine learning techniques (Page et al. 2021) or large ensembles of direct numerical simulations, are necessary.
2. A better understanding of transition should ideally lead to practical means to delay and suppress it. Some first strategies have been demonstrated in experiments and simulations (Hof et al. 2010, Kühnen et al. 2018, Marensi et al. 2020).
3. Puff decay and splitting exhibit scaling compatible with the statistics of rare (extreme) events. However, the specific physical events in puff decay and puff splitting that give rise to extreme-value behavior have not been identified. Algorithms designed to efficiently sample rare events have been applied to shear flows (Rolland 2018, 2022; Gomé et al. 2022), but not as yet to pipe flow. The relationship between puff splitting and the onset of weak slug expansion remains unclear.
4. Although there is strong evidence that the turbulent fraction decreases continuously as the critical point is approached from above (Mukund & Hof 2018), the scaling exponents and a direct connection to directed percolation remain open for pipe flow.

DISCLOSURE STATEMENT

The authors are not aware of any biases that might be perceived as affecting the objectivity of this review.

ACKNOWLEDGMENTS

The authors are very grateful to Laurette Tuckerman for her helpful comments. This work was supported by grants from the Simons Foundation (grant numbers 662985, D.B., and 662960, B.H.) and the Priority Programme "SPP 1881: Turbulent Superstructures" of the Deutsche Forschungsgemeinschaft (grant number AV120/3-2 to M.A.).

LITERATURE CITED

Agrawal N, Choueiri GH, Hof B. 2019. Transition to turbulence in particle laden flows. *Phys. Rev. Lett.* 122(11):114502

Avila K, Moxey D, de Lozar A, Avila M, Barkley D, Hof B. 2011. The onset of turbulence in pipe flow. *Science* 333(6039):192–96

Avila M, Hof B. 2013. Nature of laminar-turbulence intermittency in shear flows. *Phys. Rev. E* 87:063012

Avila M, Mellibovsky F, Roland N, Hof B. 2013. Streamwise-localized solutions at the onset of turbulence in pipe flow. *Phys. Rev. Lett.* 110(22):224502

Avila M, Willis AP, Hof B. 2010. On the transient nature of localized pipe flow turbulence. *J. Fluid Mech.* 646:127–36

Barkley D. 2011. Simplifying the complexity of pipe flow. *Phys. Rev. E* 84(1):016309

Barkley D. 2016. Theoretical perspective on the route to turbulence in a pipe. *J. Fluid Mech.* 803:P1

Barkley D, Song B, Mukund V, Lemoult G, Avila M, Hof B. 2015. The rise of fully turbulent flow. *Nature* 526(7574):550–53

Boberg L, Brosa U. 1988. Onset of turbulence in a pipe. *Z. Naturforsch. A* 43(8–9):697–726

Bottin S, Chaté H. 1998. Statistical analysis of the transition to turbulence in plane Couette flow. *Eur. Phys. J. B* 6(1):143–55

Bottin S, Daviaud F, Manneville P, Dauchot O. 1998. Discontinuous transition to spatiotemporal intermittency in plane Couette flow. *Europhys. Lett.* 43(2):171–76

Brandt L. 2014. The lift-up effect: the linear mechanism behind transition and turbulence in shear flows. *Eur. J. Mech. B* 47:80–96

Brosa U. 1989. Turbulence without strange attractor. *J. Stat. Phys.* 55(5):1303–12

Budanur NB, Dogra AS, Hof B. 2019. Geometry of transient chaos in streamwise-localized pipe flow turbulence. *Phys. Rev. Fluids* 4(10):102401

Chantry M, Tuckerman LS, Barkley D. 2017. Universal continuous transition to turbulence in a planar shear flow. *J. Fluid Mech.* 824:R1

Chapman SJ. 2002. Subcritical transition in channel flows. *J. Fluid Mech.* 451:35–97

Chen K, Xu D, Song B. 2022. Propagation speed of turbulent fronts in pipe flow at high Reynolds numbers. *J. Fluid Mech.* 935:A11

Coles D. 1962. Interfaces and intermittency in turbulent shear flow. *Méc. Turbul.* 108(108):229–50

Darbyshire A, Mullin T. 1995. Transition to turbulence in constant-mass-flux pipe flow. *J. Fluid Mech.* 289:83–114

De Lozar A, Mellibovsky F, Avila M, Hof B. 2012. Edge state in pipe flow experiments. *Phys. Rev. Lett.* 108(21):214502

Draad A, Nieuwstadt F. 1998. The earth's rotation and laminar pipe flow. *J. Fluid Mech.* 361:297–308

Drazin PG, Reid WH. 2004. *Hydrodynamic Stability*. Cambridge, UK: Cambridge Univ. Press

Duguet Y, Monokrousos A, Brandt L, Henningson DS. 2013. Minimal transition thresholds in plane Couette flow. *Phys. Fluids* 25(8):084103

Duguet Y, Pringle CC, Kerswell RR. 2008a. Relative periodic orbits in transitional pipe flow. *Phys. Fluids* 20(11):114102

Duguet Y, Willis AP, Kerswell RR. 2008b. Transition in pipe flow: the saddle structure on the boundary of turbulence. *J. Fluid Mech.* 613:255–74
Duguet Y, Willis AP, Kerswell RR. 2010. Slug genesis in cylindrical pipe flow. *J. Fluid Mech.* 663:180–208
Durst F, Ünsal B. 2006. Forced laminar-to-turbulent transition of pipe flows. *J. Fluid Mech.* 560:449–64
Eckert M. 2010. The troublesome birth of hydrodynamic stability theory: Sommerfeld and the turbulence problem. *Eur. Phys. J. H* 35(1):29–51
Eckert M. 2015. Fluid mechanics in Sommerfeld's school. *Annu. Rev. Fluid Mech.* 47:1–20
Eckhardt B, Schneider TM, Hof B, Westerweel J. 2007. Turbulence transition in pipe flow. *Annu. Rev. Fluid Mech.* 39:447–68
Faisst H, Eckhardt B. 2003. Traveling waves in pipe flow. *Phys. Rev. Lett.* 91(22):224502
Faisst H, Eckhardt B. 2004. Sensitive dependence on initial conditions in transition to turbulence in pipe flow. *J. Fluid Mech.* 504:343–52
Feynman RP, Leighton RB, Sands ML. 1963. *The Feynman Lectures on Physics*. Reading, MA: Addison-Wesley
Gibson JF, Halcrow J, Cvitanović P. 2008. Visualizing the geometry of state space in plane Couette flow. *J. Fluid Mech.* 611:107–30
Goldenfeld N, Guttenberg N, Gioia G. 2010. Extreme fluctuations and the finite lifetime of the turbulent state. *Phys. Rev. E* 81(3):035304(R)
Gomé S, Tuckerman LS, Barkley D. 2022. Extreme events in transitional turbulence. *Philos. Trans. R. Soc. A* 380:20210036
Graham MD, Floryan D. 2021. Exact coherent states and the nonlinear dynamics of wall-bounded turbulent flows. *Annu. Rev. Fluid Mech.* 53:227–53
Grebogi C, Ott E, Yorke JA. 1982. Chaotic attractors in crisis. *Phys. Rev. Lett.* 48(22):1507–10
Guckenheimer J, Holmes P. 2002. *Nonlinear Oscillations, Dynamical Systems, and Bifurcations of Vector Fields* (Applied Mathematical Sciences, No. 42). New York: Springer. 7th ed.
Hinrichsen H. 2000. Non-equilibrium critical phenomena and phase transitions into absorbing states. *Adv. Phys.* 49(7):815–958
Hof B, De Lozar A, Avila M, Tu X, Schneider TM. 2010. Eliminating turbulence in spatially intermittent flows. *Science* 327(5972):1491–94
Hof B, De Lozar A, Kuik DJ, Westerweel J. 2008. Repeller or attractor? Selecting the dynamical model for the onset of turbulence in pipe flow. *Phys. Rev. Lett.* 101(21):214501
Hof B, Juel A, Mullin T. 2003. Scaling of the turbulence transition threshold in a pipe. *Phys. Rev. Lett.* 91(24):244502
Hof B, van Doorne CW, Westerweel J, Nieuwstadt FT. 2005. Turbulence regeneration in pipe flow at moderate Reynolds numbers. *Phys. Rev. Lett.* 95(21):214502
Hof B, Van Doorne CW, Westerweel J, Nieuwstadt FT, Faisst H, et al. 2004. Experimental observation of nonlinear traveling waves in turbulent pipe flow. *Science* 305(5690):1594–98
Hof B, Westerweel J, Schneider TM, Eckhardt B. 2006. Finite lifetime of turbulence in shear flows. *Nature* 443(7107):59–62
Hogendoorn W, Poelma C. 2018. Particle-laden pipe flows at high volume fractions show transition without puffs. *Phys. Rev. Lett.* 121(19):194501
Hopf E. 1948. A mathematical example displaying features of turbulence. *Commun. Pure Appl. Math.* 1(4):303–22
Ishida T, Duguet Y, Tsukahara T. 2016. Transitional structures in annular Poiseuille flow depending on radius ratio. *J. Fluid Mech.* 794:R2
Ishida T, Duguet Y, Tsukahara T. 2017. Turbulent bifurcations in intermittent shear flows: from puffs to oblique stripes. *Phys. Rev. Fluids* 2(7):073902
Itano T, Toh S. 2001. The dynamics of bursting process in wall turbulence. *J. Phys. Soc. Jpn.* 70(3):703–16
Joseph D, Carmi S. 1969. Stability of Poiseuille flow in pipes, annuli, and channels. *Q. Appl. Math.* 26(4):575–99
Kaneko K. 1985. Spatiotemporal intermittency in coupled map lattices. *Prog. Theor. Phys.* 74(5):1033–44
Kawahara G, Uhlmann M, Van Veen L. 2012. The significance of simple invariant solutions in turbulent flows. *Annu. Rev. Fluid Mech.* 44:203–25
Kerswell R. 2018. Nonlinear nonmodal stability theory. *Annu. Rev. Fluid Mech.* 50:319–45

Klotz L, Lemoult G, Avila K, Hof B. 2022. Phase transition to turbulence in spatially extended shear flows. *Phys. Rev. Lett.* 128(1):014502
Kreilos T, Eckhardt B. 2012. Periodic orbits near onset of chaos in plane Couette flow. *Chaos* 22(4):047505
Kühnen J, Braunshier P, Schwegel M, Kuhlmann H, Hof B. 2015. Subcritical versus supercritical transition to turbulence in curved pipes. *J. Fluid Mech.* 770:R3
Kühnen J, Song B, Scarselli D, Budanur NB, Riedl M, et al. 2018. Destabilizing turbulence in pipe flow. *Nat. Phys.* 14(4):386–90
Kuik DJ, Poelma C, Westerweel J. 2010. Quantitative measurement of the lifetime of localized turbulence in pipe flow. *J. Fluid Mech.* 645:529–39
Lemoult G, Aider JL, Wesfreid JE. 2012. Experimental scaling law for the subcritical transition to turbulence in plane Poiseuille flow. *Phys. Rev. E* 85(2):025303
Lemoult G, Shi L, Avila K, Jalikop SV, Avila M, Hof B. 2016. Directed percolation phase transition to sustained turbulence in Couette flow. *Nat. Phys.* 12(3):254–58
Lindgren ER. 1957. The transition process and other phenomena in viscous flow. *Ark. Fys.* 12:1–169
Lindgren ER. 1969. Propagation velocity of turbulent slugs and streaks in transition pipe flow. *Phys. Fluids* 12(2):418–25
Lübeck S. 2004. Universal scaling behavior of non-equilibrium phase transitions. *Int. J. Mod. Phys. B* 18(31–32):3977–4118
Luchini P, Bottaro A. 2014. Adjoint equations in stability analysis. *Annu. Rev. Fluid Mech.* 46:493–517
Lustro JRT, Kawahara G, van Veen L, Shimizu M, Kokubu H. 2019. The onset of transient turbulence in minimal plane Couette flow. *J. Fluid Mech.* 862:R2
Manneville P. 2015. On the transition to turbulence of wall-bounded flows in general, and plane Couette flow in particular. *Eur. J. Mech. B* 49:345–62
Marensi E, Ding Z, Willis AP, Kerswell RR. 2020. Designing a minimal baffle to destabilise turbulence in pipe flows. *J. Fluid Mech.* 900:A31
Matas JP, Morris JF, Guazzelli E. 2003. Transition to turbulence in particulate pipe flow. *Phys. Rev. Lett.* 90(1):014501
Mellibovsky F, Eckhardt B. 2012. From travelling waves to mild chaos: a supercritical bifurcation cascade in pipe flow. *J. Fluid Mech.* 709:149–90
Mellibovsky F, Meseguer A. 2007. Pipe flow transition threshold following localized impulsive perturbations. *Phys. Fluids* 19:044102
Mellibovsky F, Meseguer A, Schneider TM, Eckhardt B. 2009. Transition in localized pipe flow turbulence. *Phys. Rev. Lett.* 103(5):054502
Meseguer A. 2003. Streak breakdown instability in pipe Poiseuille flow. *Phys. Fluids* 15(5):1203–13
Meseguer A, Trefethen L. 2003. Linearized pipe flow to Reynolds number 10^7. *J. Comput. Phys.* 186(1):178–97
Moehlis J, Faisst H, Eckhardt B. 2004. A low-dimensional model for turbulent shear flows. *New J. Phys.* 6(1):56
Monokrousos A, Bottaro A, Brandt L, Di Vita A, Henningson DS. 2011. Nonequilibrium thermodynamics and the optimal path to turbulence in shear flows. *Phys. Rev. Lett.* 106(13):134502
Moxey D, Barkley D. 2010. Distinct large-scale turbulent-laminar states in transitional pipe flow. *PNAS* 107(18):8091–96
Mukund V, Hof B. 2018. The critical point of the transition to turbulence in pipe flow. *J. Fluid Mech.* 839:76–94
Nemoto T, Alexakis A. 2021. Do extreme events trigger turbulence decay? A numerical study of turbulence decay time in pipe flows. *J. Fluid Mech.* 912:A38
Nishi M, Ünsal B, Durst F, Biswas G. 2008. Laminar-to-turbulent transition of pipe flows through puffs and slugs. *J. Fluid Mech.* 614:425–46
Noorani A, El Khoury G, Schlatter P. 2013. Evolution of turbulence characteristics from straight to curved pipes. *Int. J. Heat Fluid Flow* 41:16–26
Page J, Brenner MP, Kerswell RR. 2021. Revealing the state space of turbulence using machine learning. *Phys. Rev. Fluids* 6(3):034402
Peixinho J, Mullin T. 2006. Decay of turbulence in pipe flow. *Phys. Rev. Lett.* 96(9):094501
Peixinho J, Mullin T. 2007. Finite-amplitude thresholds for transition in pipe flow. *J. Fluid Mech.* 582:169–78
Pfenniger W. 1961. Transition in the inlet length of tubes at high Reynolds numbers. In *Boundary Layer and Flow Control, Its Principles and Applications*, ed. G Lachman, pp. 970–80. Oxford, UK: Pergamon

Philip J, Cohen J. 2010. Formation and decay of coherent structures in pipe flow. *J. Fluid Mech.* 655:258–79
Pomeau Y. 1986. Front motion, metastability and subcritical bifurcations in hydrodynamics. *Physica D* 23:3–11
Pringle CC, Kerswell RR. 2010. Using nonlinear transient growth to construct the minimal seed for shear flow turbulence. *Phys. Rev. Lett.* 105(15):154502
Pringle CC, Willis AP, Kerswell RR. 2015. Fully localised nonlinear energy growth optimals in pipe flow. *Phys. Fluids* 27(6):064102
Pringle CCT, Duguet Y, Kerswell RR. 2009. Highly symmetric travelling waves in pipe flow. *Philos. Trans. R. Soc. A* 367(1888):457–72
Pringle CCT, Kerswell RR. 2007. Asymmetric, helical, and mirror-symmetric traveling waves in pipe flow. *Phys. Rev. Lett.* 99(7):74502
Reddy SC, Schmid PJ, Baggett JS, Hennignson DS. 1998. On stability of streamwise streaks and transition thresholds in plane channel flows. *J. Fluid Mech.* 365:269–303
Reynolds O. 1883. An experimental investigation of the circumstances which determine whether the motion of water shall be direct or sinuous, and of the law of resistance in parallel channels. *Philos. Trans. R. Soc.* 174:935–82
Rinaldi E, Canton J, Schlatter P. 2019. The vanishing of strong turbulent fronts in bent pipes. *J. Fluid Mech.* 866:487–502
Riols A, Rincon F, Cossu C, Lesur G, Longaretti PY, et al. 2013. Global bifurcations to subcritical magnetorotational dynamo action in Keplerian shear flow. *J. Fluid Mech.* 731:1–45
Ritter P, Mellibovsky F, Avila M. 2016. Emergence of spatio-temporal dynamics from exact coherent solutions in pipe flow. *New J. Phys.* 18(8):083031
Rolland J. 2018. Extremely rare collapse and build-up of turbulence in stochastic models of transitional wall flows. *Phys. Rev. E* 97(2):023109
Rolland J. 2022. Collapse of transitional wall turbulence captured using a rare events algorithm. *J. Fluid Mech.* 931:A22
Rotta JC. 1956. Experimenteller Beitrag zur Entstehung turbulenter Strömung im Rohr. *Arch. Appl. Mech.* 24(4):258–81
Salwen H, Cotton FW, Grosch CE. 1980. Linear stability of Poiseuille flow in a circular pipe. *J. Fluid Mech.* 98(2):273–84
Samanta D, De Lozar A, Hof B. 2011. Experimental investigation of laminar turbulent intermittency in pipe flow. *J. Fluid Mech.* 681:193–204
Samanta D, Dubief Y, Holzner M, Schäfer C, Morozov AN, et al. 2013. Elasto-inertial turbulence. *PNAS* 110(26):10557–62
Schmid PJ. 2007. Nonmodal stability theory. *Annu. Rev. Fluid Mech.* 39:129–62
Schmid PJ, Henningson DS. 1994. Optimal energy density growth in Hagen–Poiseuille flow. *J. Fluid Mech.* 277:197–225
Schmid PJ, Henningson DS. 2001. *Stability and Transition in Shear Flows*. New York: Springer
Schneider TM, Eckhardt B, Yorke JA. 2007. Turbulence transition and the edge of chaos in pipe flow. *Phys. Rev. Lett.* 99(3):034502
Shih HY, Hsieh TL, Goldenfeld N. 2016. Ecological collapse and the emergence of travelling waves at the onset of shear turbulence. *Nat. Phys.* 12:245–48
Shimizu M, Manneville P, Duguet Y, Kawahara G. 2014. Splitting of a turbulent puff in pipe flow. *Fluid Dyn. Res.* 46(6):061403
Skufca JD, Yorke JA, Eckhardt B. 2006. Edge of chaos in a parallel shear flow. *Phys. Rev. Lett.* 96(17):174101
Song B, Barkley D, Hof B, Avila M. 2017. Speed and structure of turbulent fronts in pipe flow. *J. Fluid Mech.* 813:1045–59
Sreenivasan K, Strykowski P. 1983. Stabilization effects in flow through helically coiled pipes. *Exp. Fluids* 1(1):31–36
Takeishi K, Kawahara G, Wakabayashi H, Uhlmann M, Pinelli A. 2015. Localized turbulence structures in transitional rectangular-duct flow. *J. Fluid Mech.* 782:368–79
Tél T, Lai YC. 2008. Chaotic transients in spatially extended systems. *Phys. Rep.* 460:245–75
Trefethen LN, Trefethen AE, Reddy SC, Driscoll TA. 1993. Hydrodynamic stability without eigenvalues. *Science* 261(5121):578–84

Tuckerman LS, Chantry M, Barkley D. 2020. Patterns in wall-bounded shear flows. *Annu. Rev. Fluid Mech.* 52:343–67

van Doorne C. 2004. *Stereoscopic PIV on transition in pipe flow*. PhD Thesis, TU Delft

van Doorne CW, Westerweel J. 2009. The flow structure of a puff. *Philos. Trans. R. Soc. A* 367(1888):489–507

Waleffe F. 1995. Transition in shear flows. Nonlinear normality versus non-normal linearity. *Phys. Fluids* 7(12):3060–66

Wedin H, Kerswell RR. 2004. Exact coherent structures in pipe flow: travelling wave solutions. *J. Fluid Mech.* 508:333–71

Willis AP, Cvitanović P, Avila M. 2013. Revealing the state space of turbulent pipe flow by symmetry reduction. *J. Fluid Mech.* 721:514–40

Willis AP, Kerswell RR. 2007. Critical behavior in the relaminarization of localized turbulence in pipe flow. *Phys. Rev. Lett.* 98(1):014501

Wu X, Moin P, Adrian RJ, Baltzer JR. 2015. Osborne Reynolds pipe flow: direct simulation from laminar through gradual transition to fully developed turbulence. *PNAS* 112(26):7920–24

Wygnanski I, Champagne F. 1973. On transition in a pipe. 1. The origin of puffs and slugs and the flow in a turbulent slug. *J. Fluid Mech.* 59:281–335

Wygnanski IJ, Sokolov M, Friedman D. 1975. On transition in a pipe. 2. The equilibrium puff. *J. Fluid Mech.* 69:283–304

Xu D, Varshney A, Ma X, Song B, Riedl M, et al. 2020. Nonlinear hydrodynamic instability and turbulence in pulsatile flow. *PNAS* 117(21):11233–39

Zammert S, Eckhardt B. 2015. Crisis bifurcations in plane Poiseuille flow. *Phys. Rev. E* 91(4):041003

Annual Review of Fluid Mechanics

Volume 55, 2023

Contents

Indexes

Errata

An online log of corrections to *Annual Review of Fluid Mechanics* articles may be found at http://www.annualreviews.org/errata/fluid